Geophysical Research Letters

Supporting Information for

Stratospheric Gas-Phase Production Alone Cannot Explain Observations of Atmospheric Perchlorate on Earth

Yuk-Chun Chan [1 2], Lyatt Jaeglé [1], Pedro Campuzano-Jost [3], David C. Catling [2 4], Jihong Cole-Dai [5], Vasile I. Furdui [6], W. Andrew Jackson [7], Jose L. Jimenez [3], Dongwook Kim [3], Alanna E. Wedum [1 *], Becky Alexander [1]

[1] Department of Atmospheric Sciences, University of Washington, Seattle, WA, USA

[2] Astrobiology Program, University of Washington, Seattle, WA, USA

[3] Department of Chemistry and Cooperative Institute for Research in Environmental Sciences (CIRES), University of Colorado, Boulder, CO, USA

[4] Department of Earth and Space Sciences, University of Washington, Seattle, WA, USA

[5] Department of Chemistry and Biochemistry, South Dakota State University, Avera Health and Science Center, Brookings, SD, USA

[6] Toronto Metropolitan University, Toronto, ON, Canada

[7] Department of Civil Environmental and Construction Engineering, Texas Tech University, Lubbock, TX, USA

***** Now at Climate and Space Sciences and Engineering, University of Michigan, Ann Arbor, MI, USA

Contents of this file

Text S1. Description of the model, input datasets, and configurations we used for atmospheric perchlorate simulations.

In this study, we implement a ClO_3-Cl_2O_4-ClO_4^- chemistry scheme into version 13.3.2 of GEOS-Chem global chemical transport model (doi:10.5281/zenodo.5711194) and perform simulations of atmospheric perchlorate under the "GEOS-Chem Classic" configuration.

GEOS-Chem is a global, three-dimensional chemical transport model that is developed and maintained by an international community of scientists and engineers to study various problems in atmospheric chemistry and environmental science. The model's default configuration includes detailed chemical mechanism for simulating HO_x-NO_x-VOC-ozone-halogen-aerosol interactions in the Earth's atmosphere. The default chemical mechanism includes 649 gas-phase reactions, 97 heterogeneous reactions, and 157 photolysis reactions.

GEOS-Chem was first developed for modeling tropospheric chemistry so the modeled stratospheric chemistry in the early versions was only represented by a linearized ozone-chemistry scheme and the use of outputs from other atmospheric models as the boundary conditions in the tropopause. The Unified Tropospheric-Stratospheric Chemistry extension (UCX) mechanism, which uses a single fully coupled mechanism to represent atmospheric chemistry in both the troposphere and the stratosphere, was first implemented by Eastham et al. (2014). This development introduced stratospheric aerosols (type Ib and type II polar stratospheric clouds, as well as stratospheric sulfate), long-lived species (halocarbons and $N_2O(g)$), and the photolysis of halocarbons. The photolysis rates are computed via the Fast-JX module (Eastham et al., 2014; Neu et al., 2007). In the current version of GEOS-Chem, the emissions of long-lived halocarbons and N_2O are modeled by prescribing the planetary-boundary-layer (PBL) concentration of these species as boundary conditions.

GEOS-Chem simulations of stratospheric composition were previously evaluated against stratospheric observations by Eastham et al. (2014) and Knowland et al. (2022). We also compare the average $[O_3(g)]$, $[H_2O(g)]$, and [HCl(g)] in the stratosphere in our simulation to the observations retrieved from the measurements of Microwave Limb Sounder (MLS) on NASA's Aura satellite, finding good agreement (see Figure S2). In addition, GEOS-Chem reproduces balloon observations of [OClO(g)] in the wintertime Arctic lower stratosphere (Figure S3). The global distribution of nighttime [OClO(g)] concentrations simulated by GEOS-Chem (Figure S4) captures the broad features observed by the GOMOS stellar occultation spectrometer (Fussen et al., 2006; Tétard et al., 2013). GEOS-Chem stratospheric simulations have also been used to evaluate sulfate geoengineering (Visioni et al., 2018), to estimate the impacts of rocket launch and space debris on stratospheric chemistry (Ryan et al., 2022), and to assess the effects of a near-future supersonic aircraft fleet (Eastham et al., 2022).

Earlier versions of GEOS-Chem have been used to examine the influence of chlorine chemistry (Schmidt et al., 2016), bromine chemistry (Parrella et al., 2012;

Schmidt et al., 2016), and iodine chemistry (Sherwen et al., 2016a) on tropospheric oxidants and atmospheric mercury. The fully coupled chlorine-bromine-iodine chemistry mechanism implemented in GEOS-Chem was first described by Sherwen et al. (2016b). Recently, the modeled halogen chemistry was updated and evaluated by X. Wang et al. (2021). On a global scale, the largest sources of gas-phase inorganic chlorine, bromine, and iodine in the troposphere are acid displacement on sea-salt aerosols (i.e., HCl(g) emission from the reaction between acidic species and chloride), HOBr uptake by aerosols and cloud droplets (i.e., HOBr(g) undergoes multi-phase reactions to liberate the bromide in aerosols/cloud into the air as Br_2(g)), and the emissions of HOI(g) and I_2(g) from the ocean, respectively (X. Wang et al., 2021). The concentrations of major halogen species (HCl, BrO, and IO) in the modeled troposphere are largely consistent with the available observations (X. Wang et al., 2021).

GEOS-Chem uses a hybrid sigma-pressure grid and 72 vertical layers to represent the atmosphere from the surface to the 0.01 hPa level. Below 3 km altitude, the model layer thickness is 100-200 m, increasing to 1 km near the tropopause, and 1.5-18 km in the stratosphere. In the first 59 layers, which represent the troposphere and the stratosphere, the model has online chemistry (i.e., it solves the coupled ordinary differential equations (ODEs) for chemistry numerically to compute reaction rates and species concentrations). On average, there are 35 layers under the tropopause. In the 13 uppermost layers, the model uses a linearized ozone chemistry based on the Linoz scheme from Mclinden et al (2000), a simple high-altitude NO_y mechanism described by Eastham et al. (2014), and a set of prescribed monthly average production and loss rates of other major species from NASA's Global Modeling Initiative (GMI) chemical transport model (described in Murray et al. (2012)) to estimate the mesospheric composition.

We use the meteorological fields from Modern-Era Retrospective analysis for Research and Applications, Version 2 (MERRA2), which are produced and maintained by NASA Global Modeling and Assimilation Office (Gelaro et al., 2017), to drive our simulations. MERRA2's performance in representing the stratosphere has been evaluated (Coy et al., 2016; Wargan et al., 2017; Wargan & Coy, 2016). The parametrizations for convective transport and boundary-layer mixing used by GEOS-Chem Classic are described by Wu et al. (2007) and Lin & McElroy (2010), respectively. In each model layer, GEOS-Chem Classic uses rectilinear latitude-longitude grids and computes the advection flux of different chemical species using the TPCORE algorithm from Lin & Rood (1996).

To estimate the photochemical production of perchlorate, we add 3 species (ClO_3(g), Cl_2O_4(g), and perchlorate) and 9 gas-phase reactions (summarized in Table S1) to the existing GEOS-Chem chemical mechanism. These perchlorate-formation reactions are similar to those used in Catling et al. (2010), except that we did not include ClO_3 production via Cl(g) + O_3(g) and its loss via photolysis. Cl(g) + O_3(g) has been studied by many groups because of its importance to stratospheric ozone depletion, but the production of ClO_3(g) from the Cl+O_3 reaction has not been reported in the literature

since its early discussion in Simonaitis & Heicklen (1975). Catling et al. (2010) included Simonaitis & Heicklen (1975)'s recommended rate constants in their model and found that the rates have to be reduced by a factor of 30 to match the observations of stratospheric chlorine species. For ClO_3(g) photolysis, previous interpretation of the measurements of absorption cross sections (Goodeve & Richardson, 1937) were later shown to be incorrect (López & Sicre, 1990) and no new recommended value was given by the latest JPL evaluation report (Burkholder et al., 2020). We discuss the potential impacts of including ClO_3(g) photolysis in the model in Text S6.

In our chemistry scheme, the first step for perchlorate formation is the production of ClO_3(g) via OClO(g)+$O(^3P)$(g) (R2) or OClO(g)+O_3(g) (R3). R2 is predicted by our model to be the dominant pathway for ClO_3(g) formation. Production of $O(^3P)$(g) requires UV radiation so it increases with altitude in the stratosphere and is most active during the daytime. OClO(g) is mostly produced by ClO(g)+ BrO(g) and usually has its highest concentrations in the polar stratosphere. OClO(g) has also been detected in the tropical stratosphere (Fussen et al., 2006; Meena & Devara, 2011; Tétard et al., 2013). The rate constant for ClO_3(g) + OH(g) (R1) we use in our model is from the *ab initio* calculations done by Zhu & Lin (2001, 2003b) for the temperature range 300-3000K. We assume that the reported temperature dependence extrapolates to the colder atmospheric conditions.

$$ClO_3\,(g) + OH\,(g) + M \rightarrow HClO_4\,(g) + M \quad \text{(R1)}$$

$$OClO\,(g) + O(^3P)\,(g) + M \rightarrow ClO_3\,(g) + M \quad \text{(R2)}$$

$$OClO\,(g) + O_3\,(g) \rightarrow ClO_3\,(g) + O_2\,(g) \quad \text{(R3)}$$

We assume all the $HClO_4$(g) produced in the atmosphere converts into condensed-phase ClO_4^-(p) instantly and remains inert in aerosols. In the stratosphere, the vertical distribution ClO_4^-(p) is partly controlled by gravitational settling of aerosols. The process is parametrized using Stokes' law with a slip correction factor, and the flux is estimated using a trapezoidal scheme (Eastham et al., 2014). In the modeled troposphere, ClO_4^-(p) undergoes deposition following the parametrizations described in Liu et al. (2001) and Q. Wang et al. (2014) for wet deposition and Emerson et al. (2020) for dry deposition. We assume ClO_4^-(p) has the same deposition parameters as modeled SO_4^{2-}(p), e.g., a minimum dry deposition velocity of 0.01 cm/s, a dry deposition velocity of 0.03 cm/s over snow and ice, and an aerosol scavenging efficiency of 1.0. The source code of the modified GEOS-Chem model can be found in https://doi.org/10.5281/zenodo.7754444.

The simulation configurations are described as follows. The anthropogenic emissions of major air pollutants (e.g., NO_x(g), SO_2(g), and black carbon) are based on

the Community Emissions Data System (CEDS) inventory (Hoesly et al., 2018). The parametrization of sea-salt emissions in the model is described by Jaeglé et al. (2011). The PBL concentration of long-lived halocarbons and N_2O(g) are obtained from the WMO's 2018 Scientific Assessment of Ozone Depletion, except for CH_2Cl_2(g) and $CHCl_3$(g). For these two species, the model uses the CMIP6 observationally constrained data from Meinshausen et al. (2017). Our main simulation period is 2016 to 2018. We choose the simulation spin-up length to be 10 years, which allows the modeled stratosphere to reach steady state after we introduce the ClO_3-Cl_2O_4-ClO_4^- chemistry into the model. The 10-year-long spin-up is done by driving the simulation using 2012-2014 meteorology and emissions three times, followed by using 2015 meteorology and emissions in the final spin-up year. The native horizontal resolution of MERRA2 meteorological fields is 0.5° latitude × 0.625° longitude. Since we have to run simulations that are longer than a decade, we use a lower horizontal resolution (4° latitude × 5° longitude) so that our simulations can be completed on our machine within a reasonable time. We set the chemistry-timestep size to 30 minutes: the model updates the solar zenith angle, photolysis coefficients, and other reaction rates in each gridbox every 30 minutes in the simulation.

Text S2. Detailed description of the estimation of $\Delta^{17}O$ of modeled atmospheric perchlorate

In Text S2, we outline the method we use for calculating the modeled $\Delta^{17}O$ of perchlorate originating from photochemistry ($\Delta^{17}O(ClO_4^-$, photochemistry)). Section S2.1 briefly introduces the origin of positive ^{17}O excess ($\Delta^{17}O$) in ozone and other atmospheric species. In Section S2.2, we develop a method for predicting $\Delta^{17}O(ClO_4^-$, photochemistry) in a homogeneous photochemical-steady-state atmosphere. In Section S2.3, we assess the potential influence of other potential oxygen-exchange processes on $\Delta^{17}O(ClO_4^-$, photochemistry). In Section S2.4, we discuss the effects of atmospheric transport of oxychlorine species on $\Delta^{17}O(ClO_4^-$, photochemistry). Section S2.5 presents a synthesis on how we combine all the information and assumptions to estimate $\Delta^{17}O(ClO_4^-$, photochemistry) in the Earth's atmosphere in this study.

S2.1 Origin of Large Positive $\Delta^{17}O$ in the Atmosphere

^{17}O excess ($\Delta^{17}O \equiv \delta^{17}O - 0.52\times\delta^{18}O$) measures the enrichment of ^{17}O relative to ^{18}O that cannot be attributed to mass-dependent fractionation processes. In Earth's atmosphere, the largest source of positive $\Delta^{17}O$ is the formation of ozone via the three-body reaction between atomic oxygen and molecular oxygen (i.e., $O(^3P)(g) + O_2(g) + M \rightarrow O_3(g) + M$) (Lyons, 2001). Mass-independent fractionation occurs in this reaction because the reactive intermediates that are asymmetric (e.g., $^{17}O^{16}O^{16}O^*$ and $^{18}O^{16}O^{16}O^*$) have a longer lifetime than the symmetric ones (e.g., $^{16}O^{16}O^{16}O^*$) and thus are more likely to undergo quenching to form ozone (Hathorn & Marcus, 1999; Heidenreich &

Thiemens, 1986). The large positive $\Delta^{17}O$ in ozone is transferred to other oxygen-containing species in the atmosphere during oxidation and other oxygen-exchange processes (Thiemens, 2006). Tracking the rate of these processes and the flow of high-$\Delta^{17}O$ oxygen atoms allows for quantitative predictions about the $\Delta^{17}O$ of perchlorate originating from photochemistry ($\Delta^{17}O(ClO_4^-$, photochemistry)).

S2.2 Estimation of $\Delta^{17}O(ClO_4^-$, photochemistry) in a homogeneous photochemical-steady-state atmosphere using the rate of oxychlorine oxidation processes

To illustrate the principles we used in our estimation of $\Delta^{17}O$ of perchlorate based on the modeled photochemistry ($\Delta^{17}O(ClO_4^-$, photochemistry)), we first consider a scenario where the atmosphere is homogeneous and is in a photochemical steady state. $\Delta^{17}O$ of major oxidants (e.g., O_3, $O(^1D)$, $O(^3P)$, and OH) are spatiotemporally constant because they are in isotopic equilibrium, which is similar to assumptions made in previous work (e.g., Alexander et al., 2005, 2012). We track how oxygen atoms are introduced to oxychlorine species during their formation, starting from the lowest oxidation state, the chlorine radical (Cl(g)). Under atmospheric conditions, the main oxidation pathway that produces ClO(g) is the reaction between chlorine radical and ozone:

$$Cl(g) + O_3(g) \rightarrow ClO(g) + O_2(g)$$

The ClO molecule that forms in this reaction acquires its oxygen atom from the terminal oxygen atom of an ozone molecule ($\Delta^{17}O(O_3$, terminal)). $\Delta^{17}O(O_3$, terminal) is 50% higher than $\Delta^{17}O$ of bulk ozone ($\Delta^{17}O(O_3$, terminal) = $3/2\times\Delta^{17}O(O_3$, bulk)) because ^{17}O enrichment in ozone is contained only in the terminal oxygen atoms (Michalski & Bhattacharya, 2009). In short, the $\Delta^{17}O$ of ClO (g) immediately after formation ($\Delta^{17}O$(ClO, fresh)) should equal to $\Delta^{17}O(O_3$, terminal):

$$\Delta^{17}O(ClO, \text{fresh}) = \Delta^{17}O(O_3, \text{terminal})$$

The next stage is the formation of OClO(g) via reactions between ClO(g), BrO(g), and IO(g):

$$ClO(g) + BrO(g) \rightarrow OClO(g) + Br(g)$$
$$ClO(g) + IO(g) \rightarrow OClO(g) + I(g)$$

Similar to ClO(g), BrO(g) and IO(g) acquire their oxygen atom from the terminal oxygen of ozone in the reactions between ozone, Br(g), and I(g). This implies that $\Delta^{17}O$(OClO, fresh) should be equal to $\Delta^{17}O$(ClO), $\Delta^{17}O$(BrO), and $\Delta^{17}O$(IO):

$$\Delta^{17}O(OClO, \text{fresh}) = \Delta^{17}O(ClO)$$

In the model, $ClO_3(g)$ is produced by two oxidation pathways (R2 and R3, see Table S1). These two pathways produce $ClO_3(g)$ with different $\Delta^{17}O$ because R2 involves $O(^3P)(g)$, which carries low $\Delta^{17}O$ (≈+1.2‰), while R3 involves ozone. Two oxygen atoms in $ClO_3(g)$ are from the parent OClO molecule, while the remaining is from the oxidant. Therefore, the $\Delta^{17}O$ of $ClO_3(g)$ produced from each pathway is a weighted average of $\Delta^{17}O(OClO)$ and $\Delta^{17}O(oxidant)$:

$$\Delta^{17}O(ClO_3, R2) = 2/3\times\Delta^{17}O(OClO) + 1/3\times\Delta^{17}O(O(^3P))$$
$$\Delta^{17}O(ClO_3, R3) = 2/3\times\Delta^{17}O(OClO) + 1/3\times\Delta^{17}O(O_3, terminal)$$

$\Delta^{17}O(ClO_3, fresh)$ is calculated via the mass balance:

$$\Delta^{17}O(ClO_3, fresh) = f_{R2}\times\Delta^{17}O(ClO_3, R2) + f_{R3}\times\Delta^{17}O(ClO_3, R3)$$

where f_{R2} and f_{R3} are the fractional contribution of R2 and R3 to $ClO_3(g)$ production, respectively. For example, f_{R2} = (rate of R2)/(rate of total production of $ClO_3(g)$).

Perchlorate is produced via the reaction between $ClO_3(g)$ and OH(g) (R1). The expression for $\Delta^{17}O(ClO_4, fresh)$ is thus:

$$\Delta^{17}O(ClO_4^-, fresh) = 3/4 \times \Delta^{17}O(ClO_3) + 1/4 \times \Delta^{17}O(OH)$$

We assume that perchlorate is photochemically inert in the atmosphere and does not react with any other oxygen-containing species in the atmosphere. So we have:

$$\Delta^{17}O(ClO_4^-) = \Delta^{17}O(ClO_4^-, fresh)$$

S2.3 Potential influence of other oxygen-exchange processes on $\Delta^{17}O(ClO_4^-$, photochemistry)

In this section, we investigate whether oxygen-exchange processes other than oxidation can significantly change the $\Delta^{17}O$ of oxychlorine species after formation. In other words, we examine whether $\Delta^{17}O(ClO_x) \approx \Delta^{17}O(ClO_x, fresh)$ is a good approximation in a homogenous photochemical-steady-state atmosphere. Past laboratory studies did not observe fast oxygen exchange with water for $ClO_4^-(aq)$ and OClO(aq) (Hoering et al., 1958; Kent Murmann & Thompson, 1970), but very little is known about the oxygen-exchange reactions for oxyhalogen species in the gas phase. We focus on the oxygen-exchange reactions involving $O(^3P)(g)$ and OH(g), which have been shown to be important for $\Delta^{17}O(NO_x)$ in the stratosphere (Brinjikji & Lyons, 2021; Lyons, 2001). For example, oxygen exchange between $O(^3P)$ and NO can occur via $Q + NO \rightarrow O + NQ$, which leads to the differences between $\Delta^{17}O(NO)$ and $\Delta^{17}O(NO_2)$ in the upper

stratosphere. $\Delta^{17}O(ClO_x)$ can be lower than $\Delta^{17}O(ClO_x, \text{fresh})$ if oxychlorine species exchange oxygen with low-$\Delta^{17}O$ species at non-negligible rates relative to loss processes.

The known mechanism of OH-driven oxygen exchange involves three steps: (i) OH(g) binds with the target molecule to form an adduct, (ii) isomerization of the adduct, and (iii) dissociation of the isomerized adduct to form OH(g) and the target molecule with altered isotopic composition (Francisco, 1998; Greenblatt & Howard, 1989). Francisco (1998) studied oxygen exchange between OH and ClO via an adduct mechanism using *ab initio* methods and concluded that the rate is likely very slow and is limited by the energy barrier for hydrogen migration in HOClO adduct (Francisco, 1998). To the best of our knowledge, no study to date has explicitly estimated the rates of OH-driven oxygen exchange for BrO(g), IO(g), OClO(g), or ClO_3(g). For the HOClO adduct, the key step for isomerization is a transition state where the adduct forms a ring structure such that the hydrogen atom binds with both oxygen atoms. The existence of such O-H-O ring-structure for HOIO adduct, $HOClO_2$ adduct, and $HOClO_3$ adduct has not been predicted by existing *ab initio* studies (Begović et al., 2004; de Souza & Brown, 2014; Z.-F. Xu et al., 2003; Yang et al., 2015; R. S. Zhu & Lin, 2001). Ali & Rajakumar (2011) predicted the existence of such O-H-O ring-structure for HOBrO adduct. However, this transition state is predicted to be on a higher energy level than HO+BrO, similar to the case for HOClO described in Francisco (1998), implying that oxygen exchange via HOBrO adduct formation is likely not efficient as well. Based on available information, we argue that OH-driven oxygen exchange for BrO(g), IO(g), OClO(g), and ClO_3(g) via this adduct mechanism is likely not important under typical atmospheric conditions.

No study to date has quantified the rate of oxygen exchange between $O(^3P)$ and oxyhalogen species under atmospheric conditions to the best of our knowledge. We hypothesize that $O(^3P)$-driven oxygen exchange for oxyhalogen species is similar to that for NO and O_2 and involves two steps: (i) the atomic oxygen radical $Q(^3P)$ binds with the central halogen atom of an oxyhalogen molecule XO to form activated QXO* complex (X=Cl, Br, I, ClO, OClO; "Q" denotes ^{17}O or ^{18}O while "O" denotes ^{16}O) and (ii) QXO* dissociates into QX and O instead of undergoing quenching to form QXO(g). For ClO(g) and OClO(g), Zhu & Lin (2002, 2003a) studied their oxidation via reaction with $O(^3P)$. They estimated the rate constants for $ClO + O(^3P) + M \rightarrow OClO + M$ and $OClO + O(^3P) + M \rightarrow ClO_3 + M$ using an *ab initio* approach. We use their high-density-limit rate constants to estimate the upper limits of the rate of $O(^3P)$-driven oxygen exchange for ClO(g) and OClO(g) via our hypothesized mechanism, assuming that rate of OXO* production is similar to the rate of OXO production at high [M]. We find that the rate of OXO* (X=Cl and ClO) formation increases with altitude due to higher $[O(^3P)(g)]$. While $O(^3P)$-driven oxygen exchange for ClO(g) is likely slow compared to its other loss processes below the mesosphere, the oxygen exchange between OClO(g) and $O(^3P)$ may be important for controlling $\Delta^{17}O(OClO)$ in the upper stratosphere (Figure S5). We discuss how this hypothesized $O(^3P)$-driven oxygen exchange for OClO(g) in the upper stratosphere may affect the estimated $\Delta^{17}O(ClO_4^-)$ in Section S2.5.

S2.4 Effects of atmospheric transport of oxychlorine species on $\Delta^{17}O(ClO_4^-$, photochemistry)

In this section, we investigate whether the transport of oxidants and oxyhalogen species in the atmosphere can affect the estimation of $\Delta^{17}O(ClO_4^-$, photochemistry). To apply this method developed in Section 2.2 for estimating $\Delta^{17}O(ClO_4^-$, photochemistry) in the Earth's atmosphere, we can first estimate $\Delta^{17}O(ClO_4^-$, photochemistry) in each model gridbox and then compute a global average $\Delta^{17}O(ClO_4^-$, photochemistry) weighted by modeled perchlorate production rate in each model gridbox. A similar local-approximation method was used in Alexander et al. (2020) to calculate modeled $\Delta^{17}O(NO_3^-)$ in the troposphere and showed good performance when compared to $\Delta^{17}O(NO_3^-)$ observations.

A critical assumption we have to make for this approach is that the $\Delta^{17}O(ClO_4^-$, photochemistry) in each model gridbox can be determined using only the local information of $\Delta^{17}O$(oxidants) and oxychlorine-production rates. This local approximation works well when the photochemical lifetime of perchlorate-production–related species is much shorter than the typical timescales for atmospheric transport. In the daytime stratosphere, the photochemical lifetime of major oxidants (e.g., O_3, $O(^3P)$, OH) is shorter than 1 hour, whereas the typical timescales of stratospheric transport range from hours to months (Brasseur & Solomon, 2005). For oxyhalogen species, the predicted photochemical lifetime in the main perchlorate-producing region is also short (<1 day) compared to the typical timescales of stratospheric transport (see Figure S6). Oxyhalogen species have much longer photochemical lifetimes at night and over the poles during winter, but it should have very little influence on the estimated global average $\Delta^{17}O(ClO_4^-$, photochemistry) because the modeled production of perchlorate ceases in the absence of sunlight (Figure S6). In short, the effects of atmospheric transport of oxidants and oxychlorine species should be negligible in the estimation of the global average modeled $\Delta^{17}O(ClO_4^-$, photochemistry).

S2.5 Estimation of $\Delta^{17}O$(oxychlorine species) and $\Delta^{17}O(ClO_4^-$, photochemistry) in Earth's atmosphere

In this section, we synthesize all the information in the above sections and use the modeled $\Delta^{17}O$(oxidants) from Brinjikji & Lyons (2021) and the modeled rate of oxychlorine oxidation from our GEOS-Chem model simulation to estimate $\Delta^{17}O$(oxychlorine) and $\Delta^{17}O(ClO_4^-$, photochemistry) in the Earth's atmosphere.

Brinjikji & Lyons (2021) used a 1-D chemical kinetics model to simulate the generation of large positive $\Delta^{17}O$ during ozone formation, the transfer of $\Delta^{17}O$ between different oxidants, and the other oxygen exchange and fractionation processes in the Earth's atmosphere. We obtain the vertical profiles of the $\Delta^{17}O(O_3)$ and $\Delta^{17}O$(OH) predicted by their model from Figure 1 of their paper. $\Delta^{17}O(O_3)$ is a function of pressure and temperature during ozone formation and increases with altitude. $\Delta^{17}O$(OH) is close to

0‰ in the troposphere because of the oxygen exchange between OH(g) and tropospheric water (Dubey et al., 1997), whereas stratospheric $\Delta^{17}O(OH)$ is controlled mostly by its oxygen-exchange processes with NO(g) and NO_2(g) and is predicted to be as high as +23.4‰ (See Figure S7). While the results from Brinjikji & Lyons (2021) are largely consistent with previous modeling studies, the predicted $\Delta^{17}O(O_3)$ in the troposphere (≈+36‰) is too high compared to the more extensive measurements of $\Delta^{17}O(O_3)$ reported in recent studies (average≈+26±1 ‰) (Ishino et al., 2017; Vicars & Savarino, 2014). To better match the observations, we apply a simple correction to the modeled $\Delta^{17}O(O_3)$ and $\Delta^{17}O(OH)$:

$$\Delta^{17}O(O_3)_{corrected} = \Delta^{17}O(O_3)_{B\&J\ 2021} - 10\ ‰$$

$$\Delta^{17}O(OH)_{corrected} = (\Delta^{17}O(O_3)_{corrected}/\Delta^{17}O(O_3)_{B\&J\ 2021}) \times \Delta^{17}O(OH)_{B\&J\ 2021}$$

Figure S7 shows the vertical profiles of $\Delta^{17}O(O_3)_{corrected}$ and $\Delta^{17}O(OH)_{corrected}$. After the correction, the $\Delta^{17}O(O_3)$ in the stratosphere is reduced by 10‰ but still consistent with the observations (Krankowsky et al., 2000, 2007; Lämmerzahl et al., 2002; Mauersberger et al., 2001; Schueler et al., 1990). Brinjikji & Lyons (2021) did not show the modeled $\Delta^{17}O(O(^3P))$. We use $\Delta^{17}O(O(^3P))$=+1.2‰ at all altitudes based on the model of Zahn et al. (2006), where they assumed a rapid oxygen exchange between $O(^3P)$(g) and O_2(g). $\Delta^{17}O(O_3, terminal) = 1.5\times\Delta^{17}O(O_3)_{corrected}$, as explained in Section S2.2.

Based on the vertical profiles of $\Delta^{17}O(O_3, terminal)$, $\Delta^{17}O(OH)$, and $\Delta^{17}O(O_3)$, together with the method described in Section S2.2, we compute the estimated $\Delta^{17}O(OClO)$, $\Delta^{17}O(ClO_3)$, and $\Delta^{17}O(ClO_4^-)$ in each model gridbox. The zonal mean of estimated $\Delta^{17}O$ of these three species is shown in Figure S8. $\Delta^{17}O(OClO)$ is controlled by $\Delta^{17}O(O_3, terminal)$ and increases with altitude. $\Delta^{17}O(ClO_3)$ and $\Delta^{17}O(ClO_4^-)$ are lower than $\Delta^{17}O(OClO)$ because of the oxidants involved ($O(^3P)$(g) and OH(g)) in the oxidation processes have lower $\Delta^{17}O$ than the terminal oxygen atom in ozone. $\Delta^{17}O(ClO_3)$ and $\Delta^{17}O(ClO_4^-)$ in the troposphere are higher than the stratosphere because the reaction $OClO(g) + O_3(g) \rightarrow ClO_3(g) + O_2(g)$ becomes the major source of ClO_3(g) because of the very low $[O(^3P)(g)]$ at lower altitudes.

We estimate the average $\Delta^{17}O$ of perchlorate produced by photochemistry in the Earth's atmosphere by using the $\Delta^{17}O(ClO_4^-, photochemistry)$ and perchlorate-production rate in each model gridbox to compute a global weighted average. The result is shown in the right panel of Figure 3. Table S6 contains the numeric value, as well as the average $\Delta^{17}O(OClO)$ and $\Delta^{17}O(ClO_3)$. To examine how our estimates would change under different assumptions about $\Delta^{17}O(oxidants)$, we re-compute $\Delta^{17}O(ClO_4^-, photochemistry)$ using the uncorrected $\Delta^{17}O(O_3)$ and $\Delta^{17}O(OH)$ from Brinjikji & Lyons (2021). We find that the average $\Delta^{17}O(ClO_4^-, photochemistry)$ increases by +8.6 ‰ and further deviates from the observations of $\Delta^{17}O(ClO_4^-)$. To examine the potential influence of oxygen exchange between OClO(g) and $O(^3P)$, we hypothesize that $O(^3P)$ can erase the high $\Delta^{17}O$ in OClO(g) in the upper stratosphere and set $\Delta^{17}O(OClO) = \Delta^{17}O(O(^3P))$ above 37

km altitude (the region where the upper-limit rate of $O(^3P)$-driven oxygen exchange is higher than the rate of OClO(g) photochemical loss). In this case, the average $\Delta^{17}O(ClO_4^-$, photochemistry) reduces by about 2.2 ‰ but is still outside the observed range of $\Delta^{17}O(ClO_4^-)$. Our additional analysis demonstrates that the discrepancy between modeled $\Delta^{17}O(ClO_4^-$, photochemistry) and observed $\Delta^{17}O(ClO_4^-)$ described in the main text is robust even after changing some assumptions used in $\Delta^{17}O$ estimation.

Text S3. ClO_3-Cl_2O_4-ClO_4^- chemistry's impacts on the modeled mass budget of stratospheric chlorine

To assess the newly implemented ClO_3-Cl_2O_4-ClO_4^- chemistry's impacts on the mass budget of atmospheric chlorine in GEOS-Chem, we conduct a control experiment where ClO_3-Cl_2O_4-ClO_4^- chemistry is turned off but other configurations are identical to those in the main simulation. We then compute the differences in (i) the average vertical profiles of chlorine species (Figure S9) and (ii) total mass of these species (Table S7) between two simulations.

Figure S9 shows that the changes in the average vertical profiles of chlorine species are small. The largest changes in the average mixing ratio of major reactive chlorine species (HOCl(g), ClO(g), OClO(g)) occur between 6 to 10 km altitude. Meanwhile, the largest changes in [HCl(g)] and [$ClONO_2$(g)] are found at about 33 km altitude (see Figure S9). The magnitude of the changes is less than 0.5% at all altitudes. The changes to the total inorganic chlorine and gas-phase oxychlorine species are less than 0.2% and 0.4% throughout the atmosphere (Figure S9).

Table S7 demonstrates that ClO_3-Cl_2O_4-ClO_4^- chemistry has negligible impacts on the total mass of major chlorine species in simulations. The changes in the mass of total inorganic Cl (g/p) are less than 0.02 % (-1.9×10^{-2} % and -8.6×10^{-4} % in the stratosphere and troposphere, respectively). The largest change is seen in the total mass of tropospheric OClO(g) (–0.3%).

Text S4. Temporal variability in modeled $ClO_3(g)$ and perchlorate production

To examine the diurnal variability of different oxychlorine species, we ran a separate one-day-long simulation for 2016/01/01 and archived the model outputs at hourly resolution.

Figure S10 shows the diurnal cycle of $ClO_3(g)$ production in the stratosphere in the simulation for 2016/01/01. During the daytime, the model predicts that $ClO_3(g)$ production via OClO+O is 2 to 3 orders of magnitude higher than the $OClO+O_3$ pathway. $OClO+O_3$ is the dominant pathway during the nighttime but has a much smaller overall contribution to ClO_3 (g) production. Globally, we find that $OClO+O_3$ contributes only 3% to $ClO_3(g)$ production in the stratosphere on average.

The diurnal cycle of ClO_3 production via OClO+O is mostly driven by [$O(^3P)$] but not [OClO(g)] (See Figure S10). While OClO undergoes photolysis quickly during the daytime, the formation rate of OClO via ClO + BrO is also high because ClO and BrO are daytime species. Therefore, the model still predicts a moderate amount of OClO during the daytime (~ a factor of 10 lower than the nighttime values over the tropics). In contrast, atomic oxygen formation completely shuts down during the nighttime – nighttime [$O(^3P)$ (g)] is more than 2 orders of magnitude lower than the daytime peak. This explains why the model predicts more active ClO_3 production during the daytime and over the tropics/ high latitudes in summertime.

Gas-phase production of perchlorate in the stratosphere is also more active during the daytime because the reaction requires OH(g) (Figure S11). The model predicts that the diurnal cycle of modeled perchlorate production is mostly driven by [OH(g)] (Figure S11).

Figure S12 shows the seasonal and interannual variability of modeled perchlorate production in the stratosphere. Although higher [$ClO_3(g)$] can be found in the wintertime polar stratosphere due to elevated [ClO(g)] near polar vortices, the seasonal cycle of perchlorate production at high latitudes is still mostly driven by [OH(g)]. Gas-phase production of perchlorate in the tropical stratosphere is active throughout the year and shows very little seasonal variability (Figure S12).

Text S5. Description of Mann–Whitney U test and the analysis of difference in near-surface [ClO_4^- (p)]

Considering the non-negligible fraction of under-detection-limit measurements and the uncertainty in the statistical distribution of [ClO_4^- (p)], we perform Mann-Whitney U tests to analyze whether the difference between observations and model predictions is statistically significant. The Mann-Whitney U test is a nonparametric test that uses the ranks instead of raw values to assess whether the population of two groups are the same. A more detailed description on the applications of the Mann-Whitney U test for analyzing environmental data that has under-detection-limit measurements can be found in the Chapter 9 of Helsel (2013).

In each comparison, we first sort the observation data (X_1, X_2, ... X_n, n = number of measurements) and model data (Y_1, Y_2, ... Y_m, m = number of measurements) together and compute their ranks (x_1, x_2, ... x_n, y_1, y_2, ... y_m). All the values under the detection limit (regardless of whether they are observations and model predictions) are assigned the same rank. The joint ranks are then used to compute the Mann-Whitney U statistic:

$$U = \sum_{i=1}^{n}\sum_{j=1}^{m} S(x_i, y_j)$$

where S = 1 when $x_i > y_j$, S = 0.5 when $x_i = y_j$, and S = 0 when $x_i < y_j$.

The U statistic can then be used to test whether we can reject the null hypothesis that the probability of observations being larger than model predictions is equal to the probability of model predictions being larger than observations (i.e., model predictions' population is not distinct from that of observations). The alternative hypothesis is that observations and model predictions do not have the same population. In this study, we use Python Scipy package's stats.mannwhitneyu function to compute the Mann-Whitney U statistics and the corresponding p-values. All the test results can be found in Table S8.

Text S6. Description of ClO_3 photolysis model sensitivity experiment

To date, laboratory measurements of ClO_3(g) absorption cross-section are still inconsistent with each other (Burkholder et al., 2020; Wayne et al., 1995). The absorption spectrum measured by Goodeve & Richardson (1937) were later attributed to the absorption of Cl_2O_6 (g) (López & Sicre, 1990). Willner and coworkers used $FOClO_3$ to generate ClO_3 and measured its absorption cross-section in neon matrix. ClO_3 shows two broad absorption bands at the wavelength of 240-700 nm in their experimental set-ups (Grothe & Willner, 1994; Kopitzky et al., 2002). Several other groups used flow-tube experiments to measure the absorption spectrum of the O+OClO reaction product, which is expected to be ClO_3(g) (Green et al., 2004; Mauldin III et al., 1997). They observed spectra with a shape that is very different to that estimated by Willner and coworkers. In particular, they did not observe the visible absorption band that centered at 432 nm suggested by Willner and coworkers. Domae et al. (2014) measured the absorption cross-section of ClO_3 in aqueous phase. They generated ClO_3(aq) via the radiolysis of chlorate solution. They observed an absorption band that centered at 330 nm (red-shifted compared to Kopitzky et al. (2002)'s observed UV band) and a peak absorption cross-section of 1.8×10^{-17} cm^2 (about 7 times higher than the peak absorption cross-section of Kopitzky et al. (2002)'s observed UV band).

We conduct two model sensitivity experiments to estimate the potential impacts of ClO_3 photolysis on perchlorate production. We use the smoothed UV/visible absorption spectrum from Kopitzky et al. (2002) (described in text and shown in their Figure 9; also see our Figure S13). In the first experiment, we consider only the UV absorption band that centers at 311.5 nm (Figure S13). In the second experiment, we consider the whole absorption spectrum. We implement these two versions of ClO_3 photolysis into the current model and run one-year-long simulations for 2016. We assume a quantum yield of 1 at all wavelengths and the photolysis products to be OClO(g) and $O(^3P)$(g). We use the 2016/01/01 concentration fields from the main simulation as initial conditions.

Figure S14 compares the modeled zonal average perchlorate production in 2016 with and without ClO_3 photolysis. The spatial pattern of modeled perchlorate production in ClO_3-photolysis simulations is similar to that in the main simulation. Globally, perchlorate production is reduced by a factor of 6 when only the 311.5-nm-centered absorption spectrum is considered. When the whole absorption spectrum is considered, global perchlorate production is reduced by a factor of 31 (see Table S9).

Kopitzky et al. (2002) used ClO(g) absorption to calibrate the measurements of the absolute absorption cross-section of ClO_3(g), which would be affected by the assumed quantum yield of ClO(g) production. Given this calibration uncertainty and the fact that Kopitzky et al. (2002)'s finding has not been reproduced by other research groups yet, we assign an extra factor of 2 to the range of the estimated impact of ClO_3 photolysis on perchlorate production, hence the factor of 3-61 reduction that we are reporting in the revised main text.

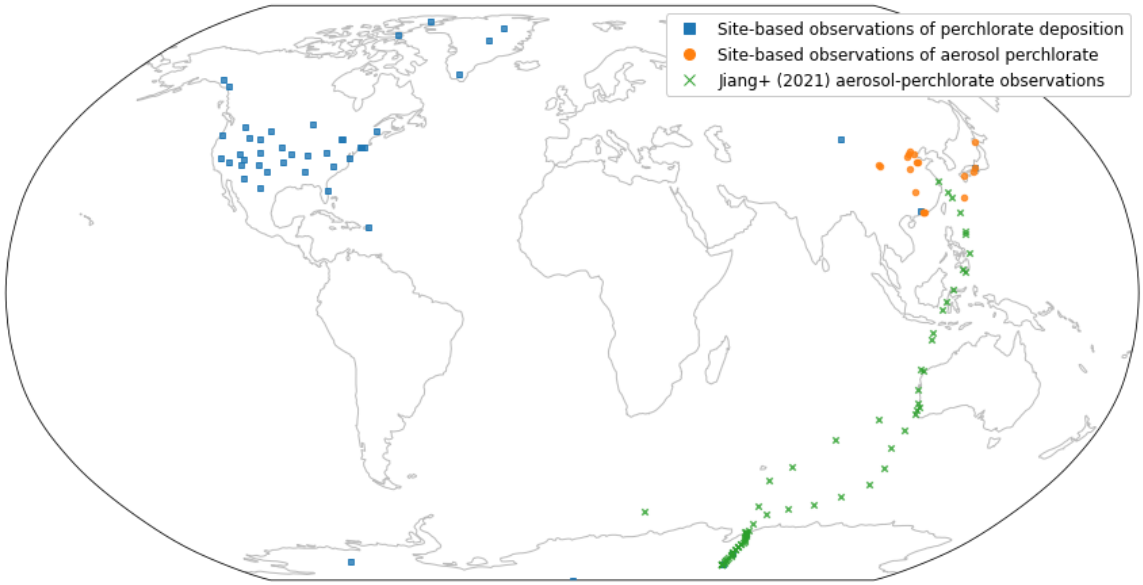

Figure S1. Geographic location of the near-surface observations of atmospheric perchlorate reported in the literature.

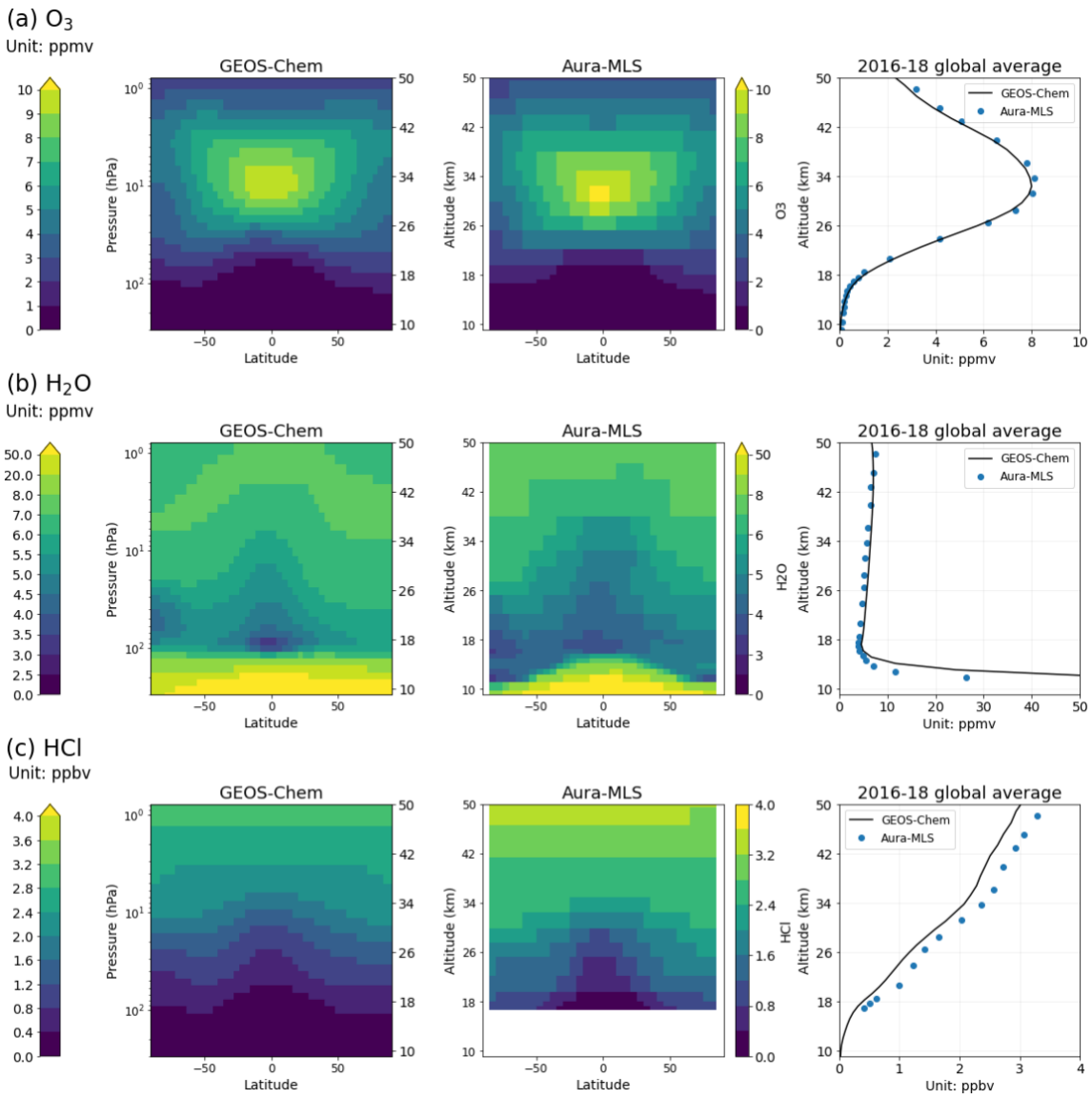

Figure S2. Comparison of modeled and observed average volume mixing ratios of stratospheric (a) ozone, (b) water vapor, and (c) HCl (g). We obtain the Aura Microwave Limb Sounder (Aura-MLS) data from the dataset of monthly average stratospheric composition measurements compiled by Hegglin et al. (2021) (https://doi.org/10.5281/zenodo.4265393).

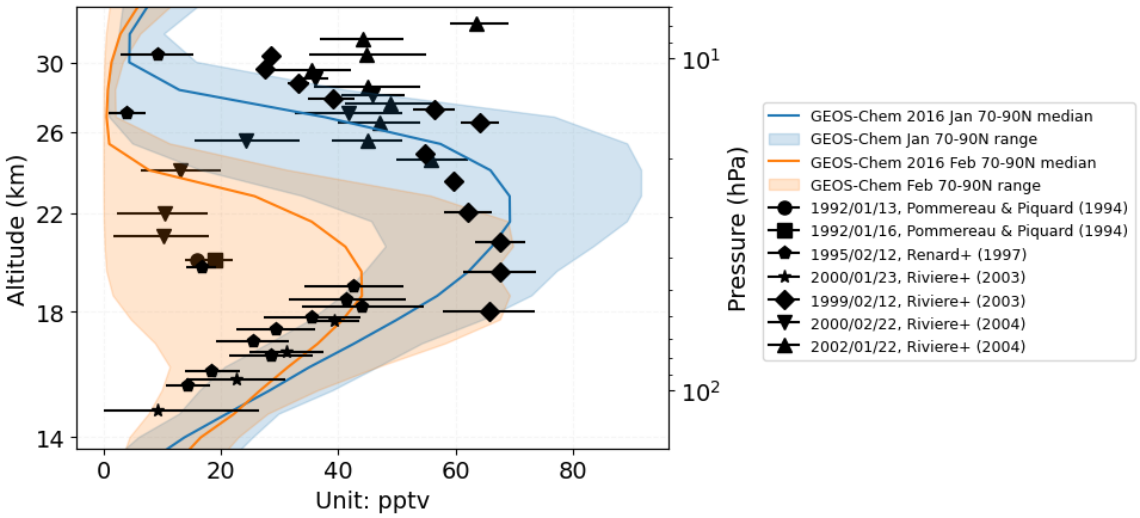

Figure S3. Comparison of the vertical profiles of nighttime OClO volume mixing ratios in the wintertime Arctic in our simulation and reported in situ observations. The observations were done by balloon-borne instruments during different field campaigns (Pommereau & Piquard, 1994; Renard et al., 1997; Rivière et al., 2003, 2004). All these field campaigns were stationed near Kiruna, Sweden (67.9°N, 20.2°E). The modeled profiles are showing the statistics of the daily 9-to-11-pm average The error bars are showing the reported measurement uncertainty. [OClO (g)] over 70°-90° N in the simulation for January and February 2016. The model range includes both the spatial and temporal variability.

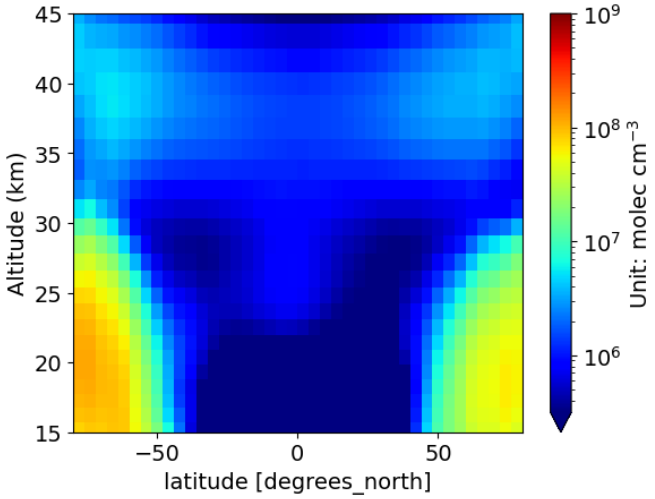

Figure S4. Estimates of annual average nighttime OClO concentration (unit: molec cm^{-3}) from the simulation for 2016. We use the daily 9-to-11-pm (local time) average [OClO (g)] from the simulation to compute the annual nighttime average, after removing the data points with solar zenith angle<120°. Figure S4 can be compared to Figure 8 in Tétard et al. (2013) (link: https://doi.org/10.5194/amt-6-2953-2013).

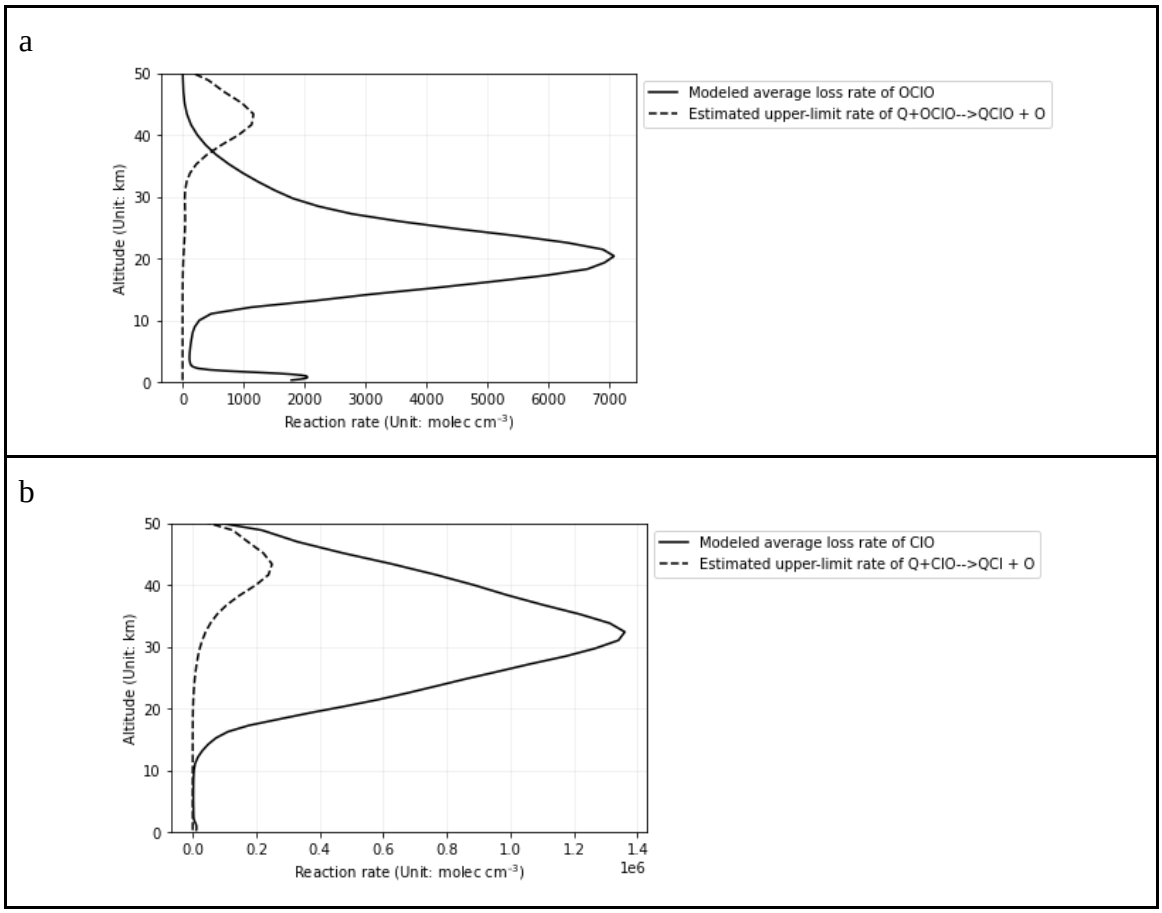

Figure S5. Modeled average loss rate and estimated upper-limit rate of O(3P) driven oxygen exchange for (a) ClO and (b) OClO. We use "Q" to denote 17O or 18O and "O" to denote 16O. The upper-limit rate of Q+ClO→ QCl+O is computed by multiplying the high-density-limit rate constant from Zhu and Lin (2003a) ($\boldsymbol{k(T)} = \boldsymbol{4.33 \times 10^{-11}\, T^{-0.03} e^{43/T}}$), average modeled [O(g)] and [ClO(g)], and a factor of 1/2 (assuming the probability of breaking either Cl-O bond in QClO* is the same). The upper-limit rate of Q+OClO → QClO + O is computed by multiplying the high-density-limit rate constant from the JPL Chemical Kinetics and Photochemical Data for Use in Atmospheric Studies Evaluation Number 19 ($\boldsymbol{k = 8.3 \times 10^{-12}}$), average modeled [O(g)] and [ClO(g)], and a factor of 1/3 (assuming the probability of breaking any of the three Cl-O bonds in QClO2* is the same).

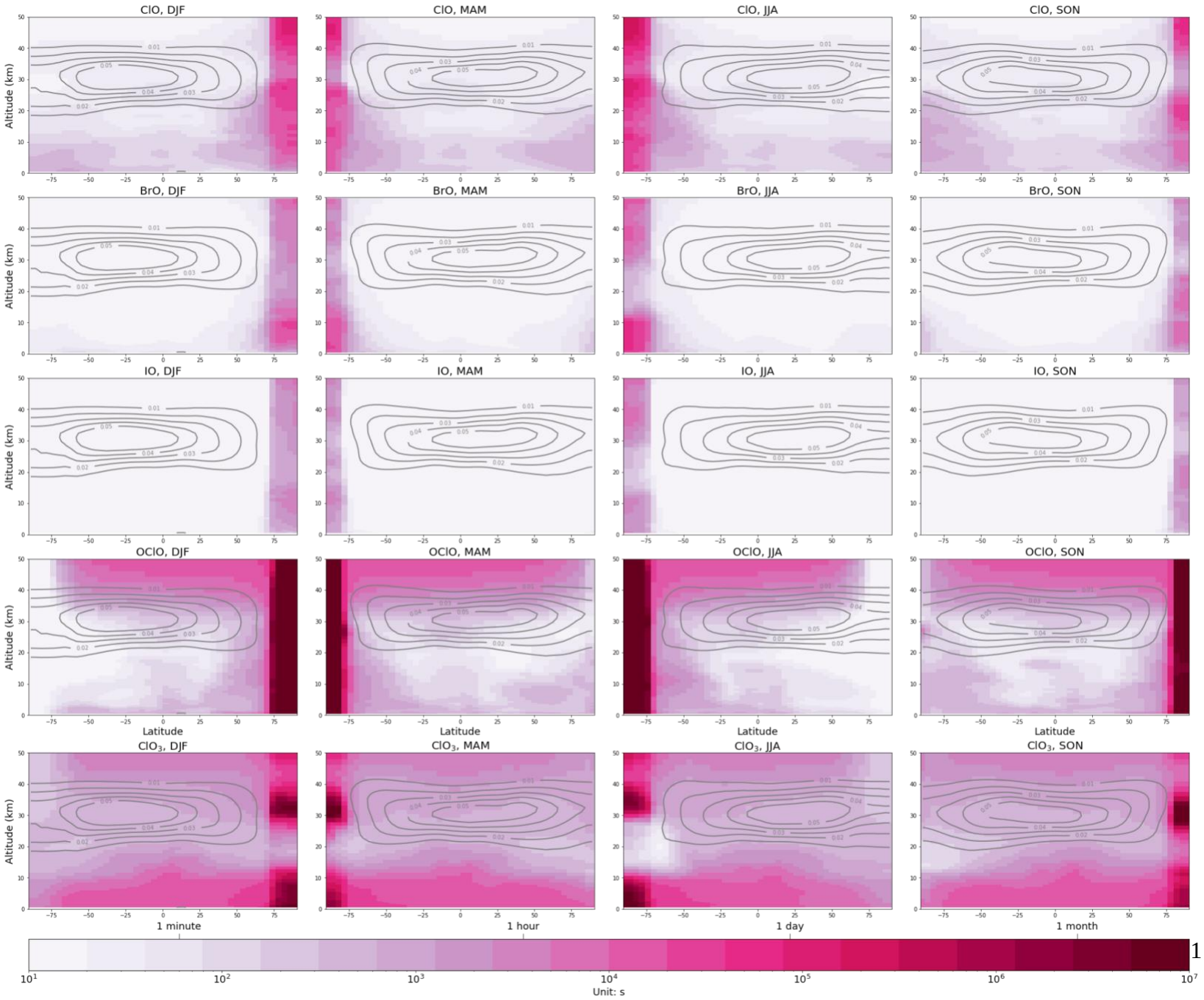
ClO, DJF
ClO, MAM
ClO, JJA
ClO, SON
BrO, DJF
BrO, MAM
BrO, JJA
BrO, SON
IO, DJF
IO, MAM
IO, JJA
IO, SON
OClO, DJF
OClO, MAM
OClO, JJA
OClO, SON
ClO3, DJF
ClO3, MAM
ClO3, JJA
ClO3, SON
Altitude (km)
Latitude
1 minute
1 hour
1 day
1 month
Unit: s

Figure S6. Modeled average photochemical lifetime (=concentration/ loss rate) of ClO(g), BrO(g), IO(g), OClO(g), and ClO_3(g) in different seasons (color-filled contours, unit: ‰) overlaying with average perchlorate-production rate (gray contours, unit: molecule cm^{-3} s^{-1}).

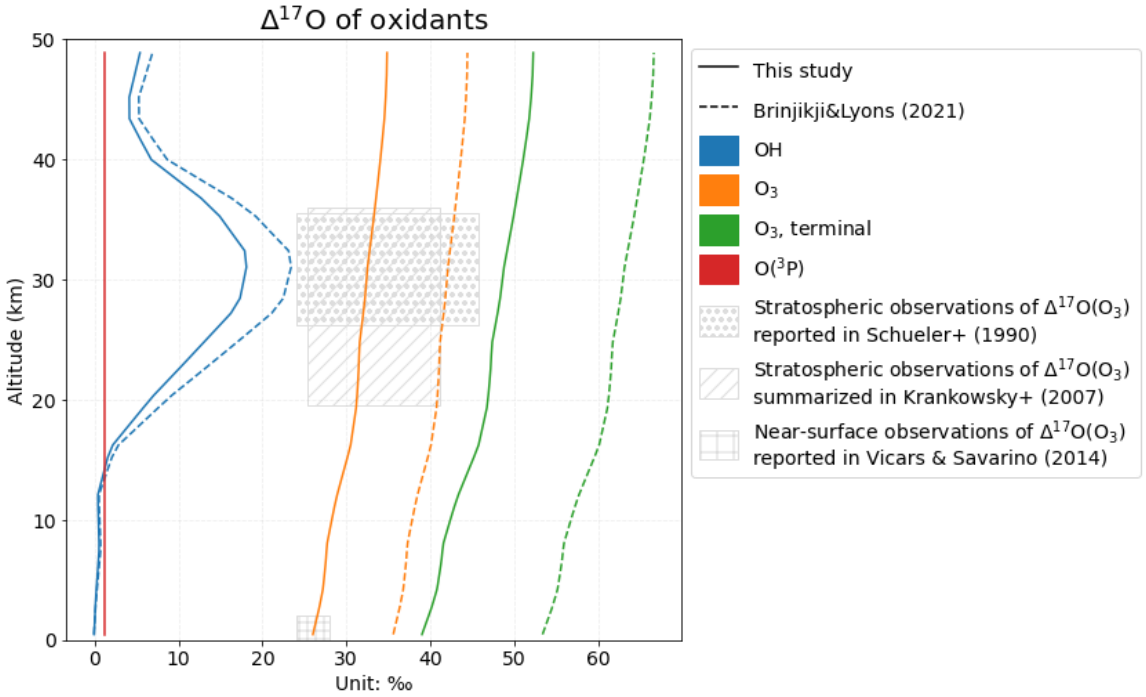

Figure S7. Vertical profiles of $\Delta^{17}O(O_3)$, $\Delta^{17}O(O_3$, terminal), $\Delta^{17}O(OH)$, and $\Delta^{17}O(O(^3P))$. The hatched boxes for stratospheric observations of $\Delta^{17}O(O_3)$ indicates the ranges of measured $\Delta^{17}O(O_3)$ and sampling altitudes reported in Schueler et al. (1990), Krankowsky et al. (2000, 2007), Mauersberger et al. (2001), and Lämmerzahl et al. (2002). Observations of the latter four studies were summarized in Table 1 of Krankowsky et al. (2007). The hatched box for near-surface observations of $\Delta^{17}O(O_3)$ indicates the range of measurements of $\Delta^{17}O(O_3)$ in the samples collected by the Research Vessel (R/V) Polarstern in the Atlantic Ocean at different latitudes (53.2°S to 53.5°S) (Vicars & Savarino, 2014).

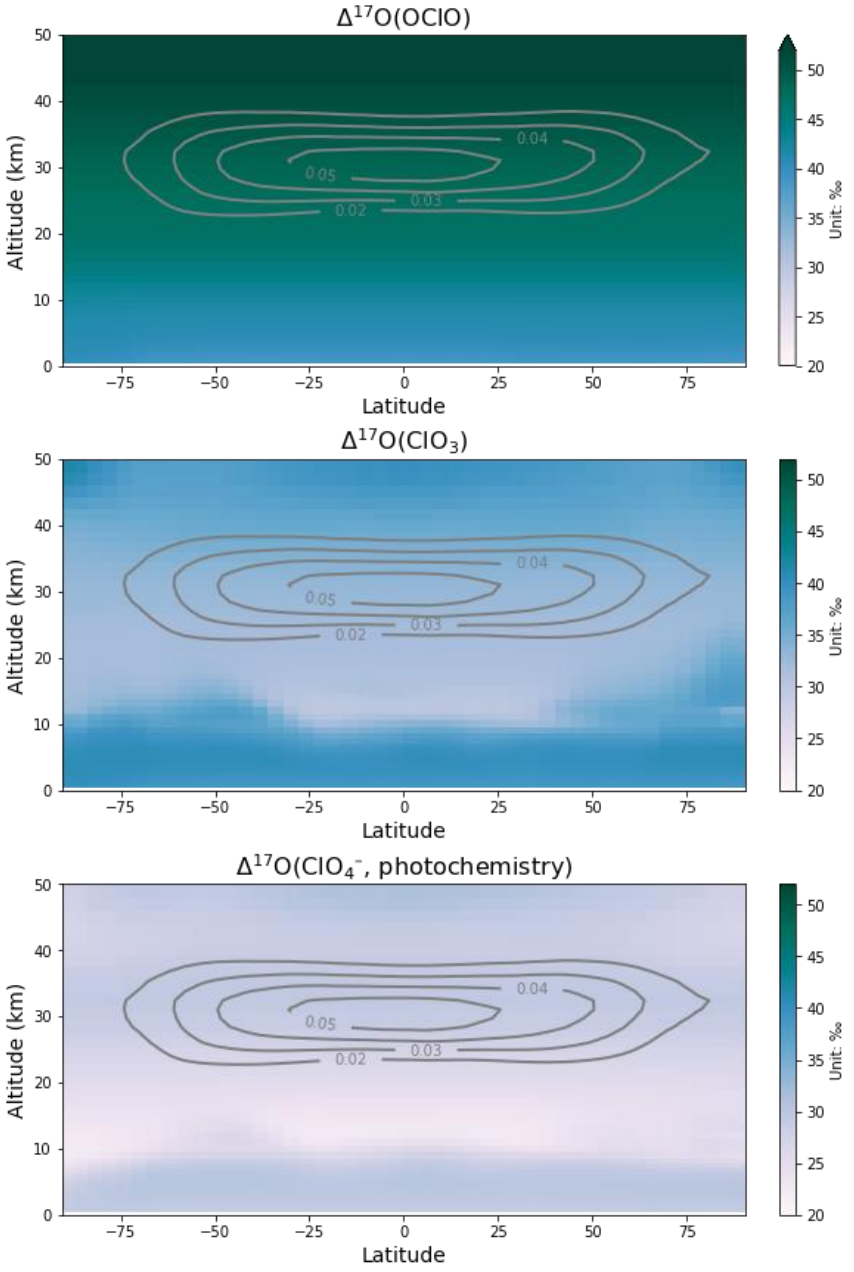

Figure S8. Zonal average of estimated $\Delta^{17}O(OClO)$, $\Delta^{17}O(ClO_3)$, and $\Delta^{17}O(ClO_4^-)$ (color-filled contour, unit: ‰) overlaying with average perchlorate-production rate (gray contours, unit: molecule cm^{-3} s^{-1}).

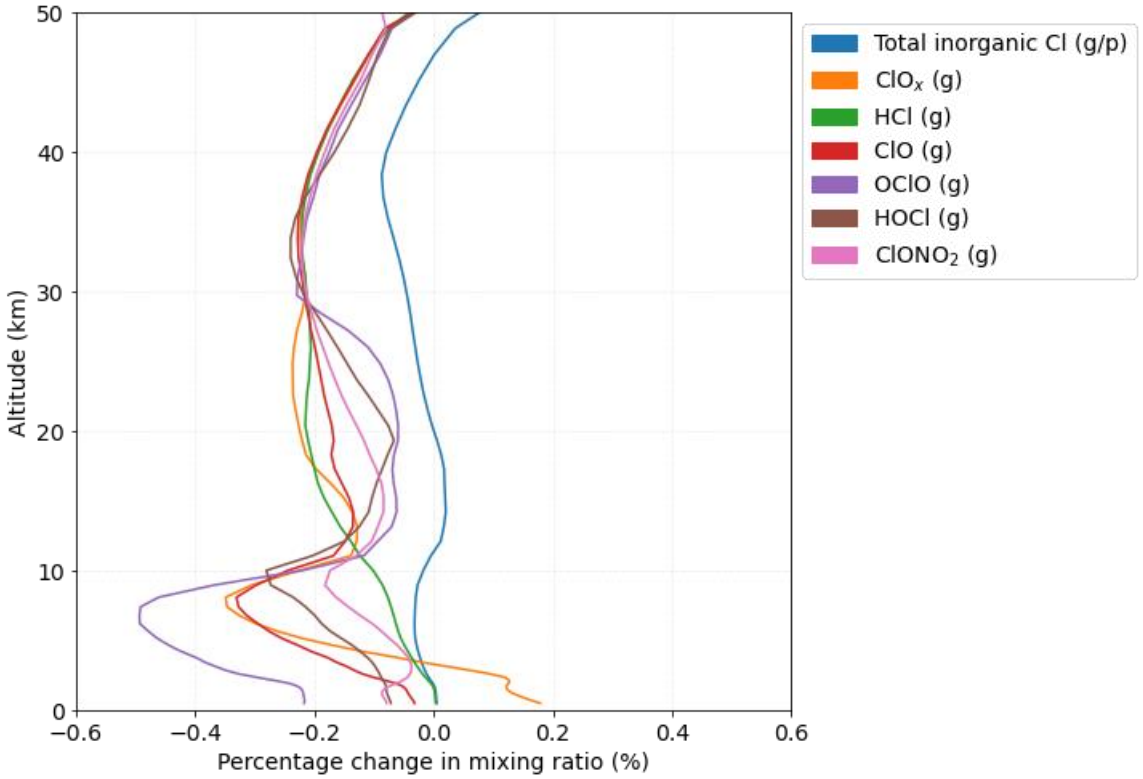

Figure S9. Vertical profiles of the changes in global average mixing ratio of different chlorine species after the implementation of ClO_3–Cl_2O_4–ClO_4^- chemistry. "Total inorganic Cl" refers to the sum of all modeled inorganic chlorine chemical species (Total inorganic Cl (g/p) ≡ HCl (g) + $ClONO_2$ (g) + HOCl (g) + ClO (g) + OClO (g) + ClOO (g) + 2×Cl_2 (g) + Cl (g) + BrCl (g) + ICl (g) + $ClNO_2$ (g) + 2×Cl_2O_2 (g) + 2×Cl_2O_4 (g) + Cl^-(p) + ClO_4^-(p)). ClO_x (g) refers to the gas-phase inorganic oxychlorine chemical family (ClO_x (g) ≡ ClO (g) + OClO (g) + ClOO (g) +ClO_3 (g) + 2×Cl_2O_2 (g) + 2×Cl_2O_4 (g)).

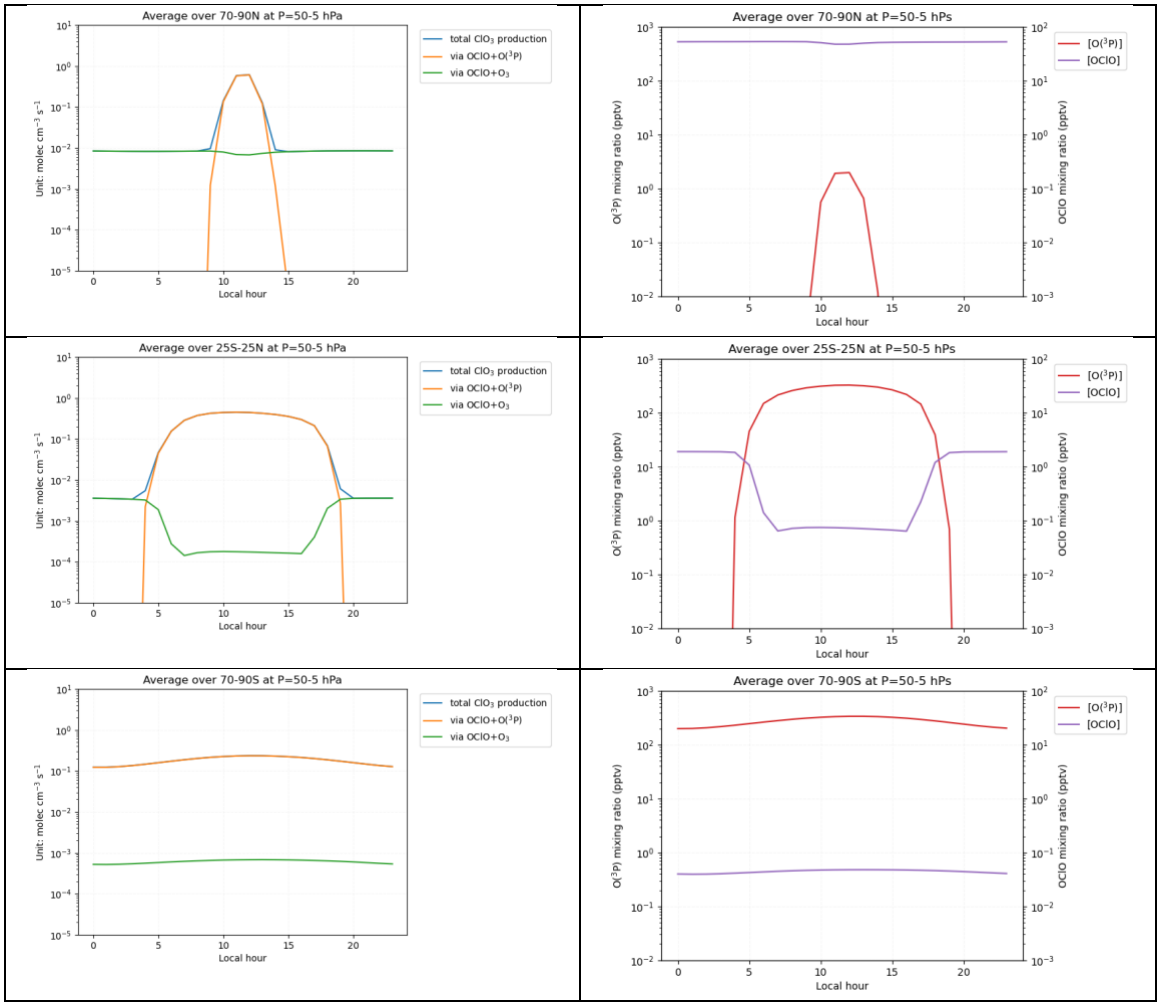

Figure S10. Diurnal cycle of ClO_3(g) production via OClO+O and OClO+O_3 pathway (on the left) and volume mixing ratios of $O(^3P)$(g) and OClO(g) (on the right) averaged over different latitudes (70°-90°N, 25°S-25°N, and 70°-90°S) at P=50-5 hPa in the simulation for 2016/01/01.

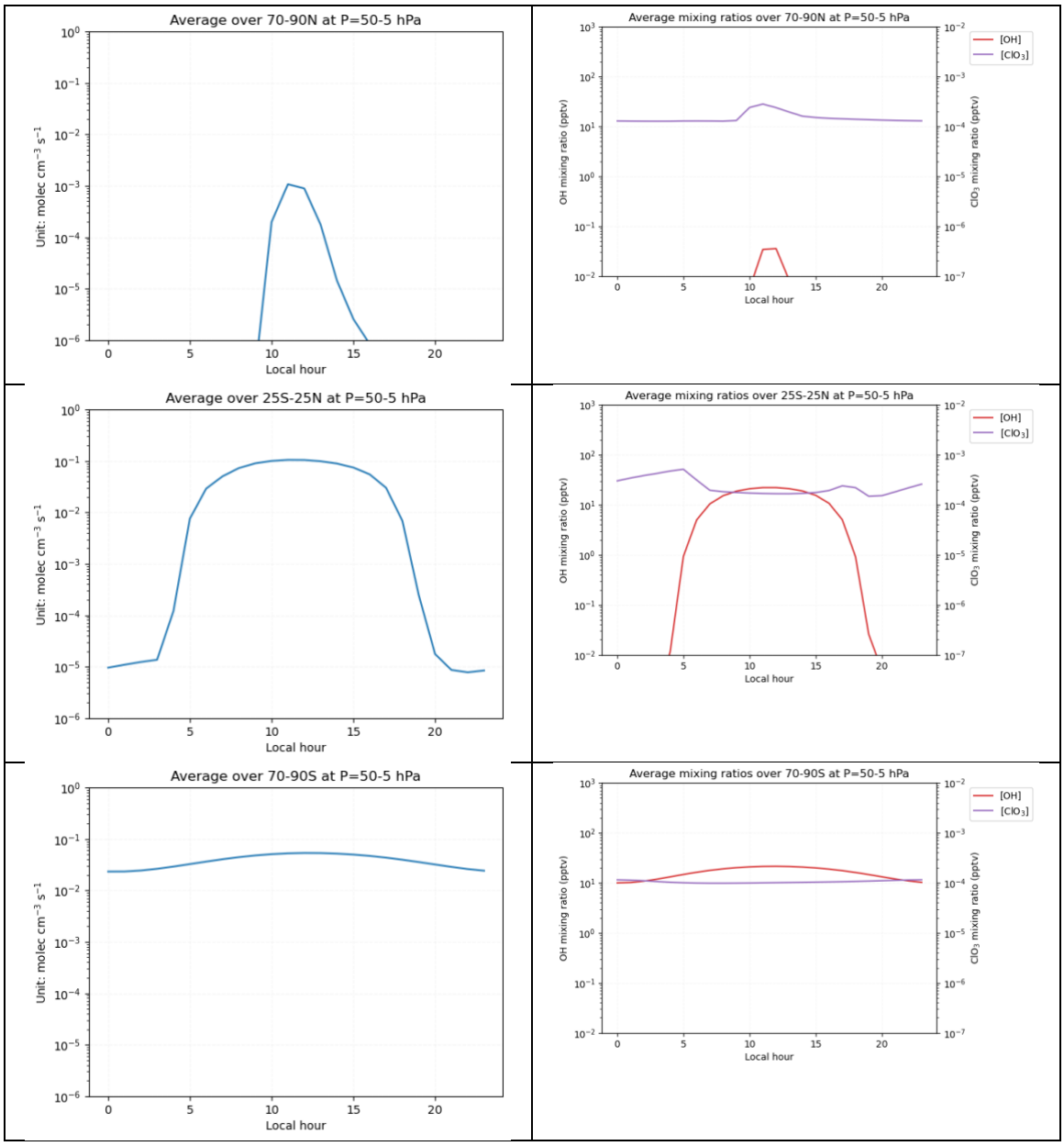

Figure S11. Diurnal cycle of gas-phase production of perchlorate (on the left) and volume mixing ratios of ClO_3(g) and OH(g) (on the right) averaged over different latitudes (70°-90°N, 25°S-25°N, and 70°-90°S) at P=50-5 hPa in the simulation for 2016/01/01.

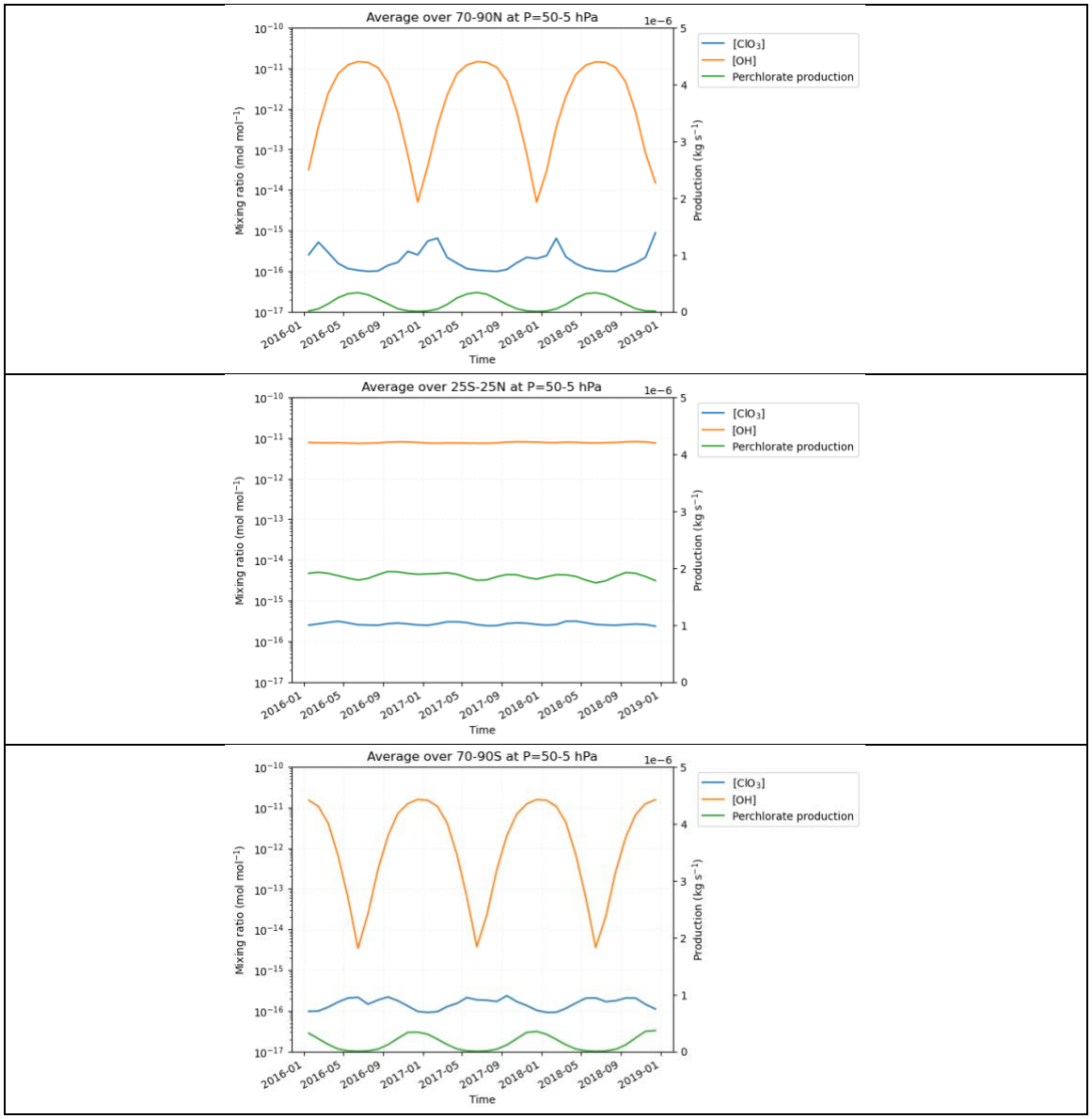

Figure S12. Modeled gas-phase production of perchlorate (on the left) and volume mixing ratios of $O(^3P)(g)$ and OClO(g) (on the right) averaged over different latitudes (70°-90°N, 25°S-25°N, and 70°-90°S) at P=50-5 hPa in each month during the simulation period (2016-2018).

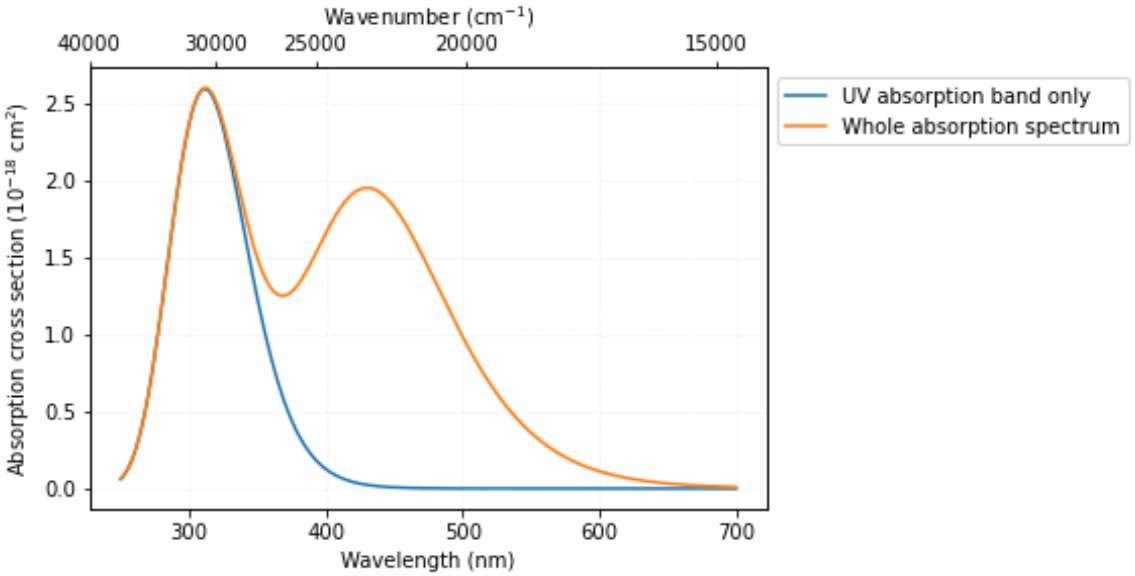

Figure S13. ClO_3 absorption spectra that we adapted from Kopitzky et al. (2002) (described in their main text and shown in their Figure 9) and use for the ClO_3-photolysis model sensitivity experiment.

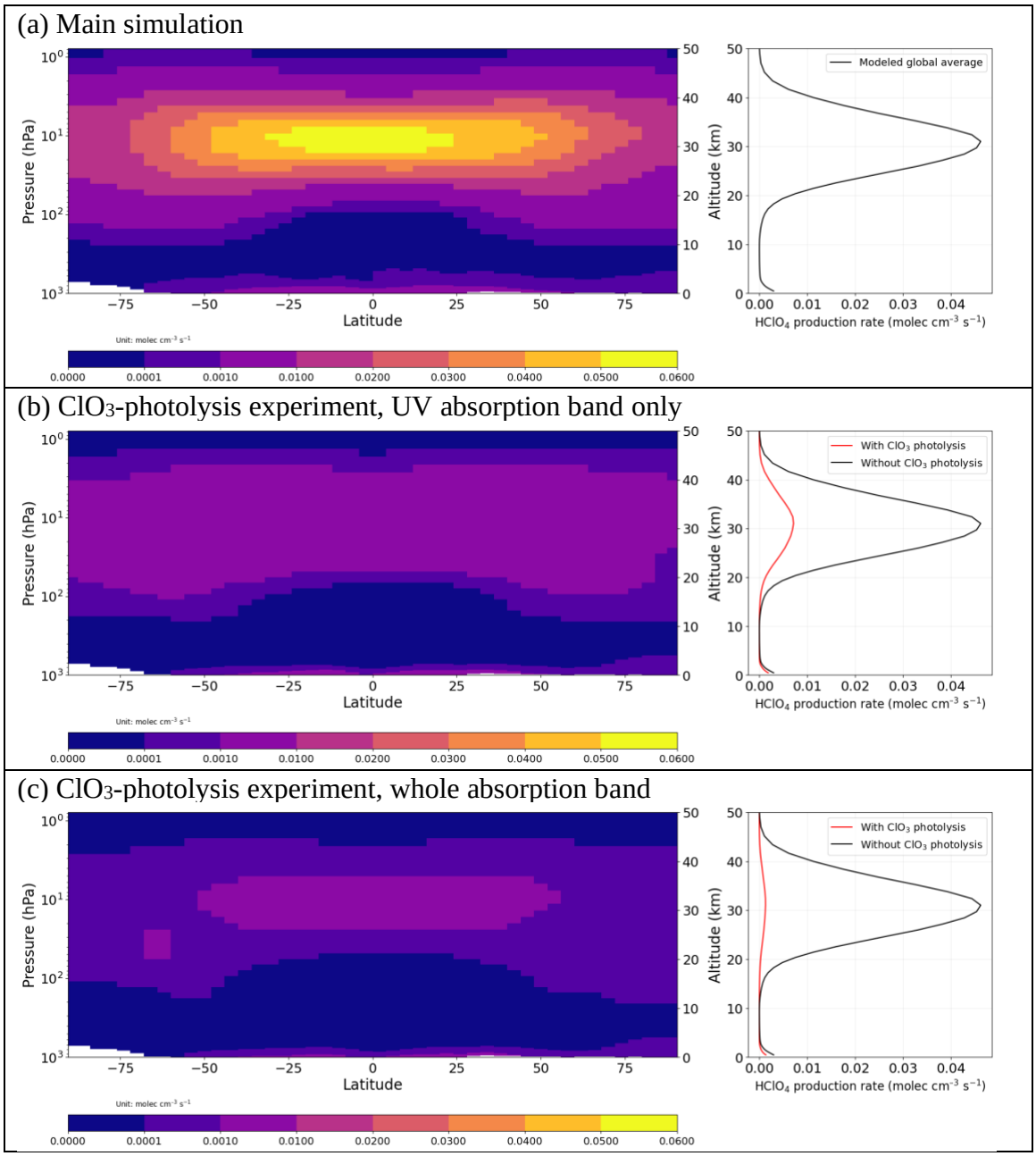

Figure S14. Average perchlorate production rate in the modeled stratosphere and troposphere in 2016 from (a) the main simulation, (b) the ClO_3-photolysis experiment where we consider only the UV absorption band that centers at 311.5 nm from Kopitzky et al. (2002), and (c) the ClO_3-photolysis experiment where we consider the whole absorption band from Kopitzky et al. (2002).

Table S1. Summary of gas-phase reactions used in GEOS-Chem for perchlorate simulations.

Reaction number	Reactants	Products	Rate constants	Reference(s)
Three-body reactions (Rate-constant units: cm^6 $molecules^{-2}$ s^{-1} for $k_0(T)$, cm^3 $molecules^{-1}$ s^{-1} for $k_\infty(T)$)				
R1	$ClO_3 + OH + M$	$HClO_4 + M$	$k_0(T) = 3.13 \times 10^{-24} \left(\frac{300}{T}\right)^{10.4} e^{\frac{-2201}{T}}$ $k_\infty(T) = 4.77 \times 10^{-10} \left(\frac{300}{T}\right)^{-0.07} e^{\frac{-25}{T}}$	Zhu & Lin (2003b)
R2	$OClO + O(^3P) + M$	$ClO_3 + M$	$k_0(T) = 2.9 \times 10^{-31} \left(\frac{300}{T}\right)^{3.1}$ $k_\infty(T) = 8.3 \times 10^{-12}$	JPL-19-5
R4	$ClO + ClO_3 + M$	$Cl_2O_4 + M$	$k_0(T) = 8.1 \times 10^{-27} \left(\frac{300}{T}\right)^{10.2} e^{\frac{-1597}{T}}$ $k_\infty(T) = 2.44 \times 10^{-10} \left(\frac{300}{T}\right)^{-0.094} e^{\frac{-82}{T}}$	Xu & Lin (2003)
Two-body reactions (Rate-constant unit: cm^3 $molecules^{-1}$ s^{-1})				
R3	$OClO + O_3$	$ClO_3 + O_2$	$k(T) = 2.1 \times 10^{-12} e^{\frac{-4700}{T}}$	JPL-19-5
R5	$ClO_3 + OH$	$OClO + HO_2$	$k(T) = 3.51 \times 10^{-10} \left(\frac{300}{T}\right)^{-0.09} e^{\frac{-18}{T}}$	Zhu & Lin (2001)
R6	$ClO + ClO_3$	$OClO + ClOO$	$k(T) = 8.22 \times 10^{-13} \left(\frac{300}{T}\right)^{-2.28} e^{\frac{-2417}{T}}$	Xu & Lin (2003)
R7	$ClO + ClO_3$	$2OClO$	$k(T) = 2.39 \times 10^{-13} \left(\frac{300}{T}\right)^{-2.11} e^{\frac{-2870}{T}}$	Xu & Lin (2003)
Photolysis reactions				

R8	Cl_2O_4 + hν	2OClO	Absorption cross-section from JPL-19-5. Average photolysis coefficient at 30 km altitude is 6.9×10^{-5} (s^{-1}) over the tropics (30°S-30°N).	JPL-19-5

Notes:

$k_\infty\ (T)$ is the high-density-limit rate constant for the three-body reaction at temperature *T*.
$k_0\ (T)[M]$ is the low-density-limit rate constant for the three-body reaction at temperature *T* and air number density [*M*].
Three-body reaction rate constant *k* at temperature *T* and air number density $M\ =$

$$\left(\frac{k_\infty(T)k_0(T)[M]}{k_\infty(T)+k_0(T)\ [M]}\right)\ 0.6^{\left(1+\left[log_{10}\left(\frac{k_0(T)\ [M]}{k_\infty(T)}\right)\right]^2\right)^{-1}}$$

JPL-19-5 refers to the JPL Chemical Kinetics and Photochemical Data for Use in Atmospheric Studies Evaluation Number 19 (Burkholder et al., 2020).

Table S2. Summary of observations of perchlorate in tropospheric aerosols during non-fireworks periods reported in different studies

Study	Geographic location	Site type	Lat (°)	Long (°)	Sampling period	Study reported clear fireworks influence? (Y/N)	Sampling Freq.	Aerosol size bins	Detection limit (ng m^{-3})	# Obs	# Detect	Mean (ng m^{-3})	S.D. (ng m^{-3})	Min. (ng m^{-3})	Median (ng m^{-3})	Max. (ng m^{-3})
Yamada et al. (2009, 2012)	Kyoto, Japan	U	35.050	135.780	2006 Jun - 2010 Jan	N	Daily	PM4	1.33E-02	131	131	6.2E-01	1.32E+00	2E-02	2.5E-01	9.64E+00
Handa et al. (2010)	Okinawa, Japan	B	26.870	128.260	2005 Aug 15 - 2006 Oct 31	N	Weekly	PM45	6E-02	60	37	N/A	N/A	N/A	1.07E-01	1.8E+00
Y. Shi et al. (2011)	Lanzhou, China	U	36.052	103.839	2007 Feb 01 - 2007 Mar 04	Y	12 hours	PM10, PM10-100	5.56E-03	25	25	2.71E+00	2.03E+00	3E-02	1.98E+00	6.9E+00
	Yuzhong County, China	R	35.570	104.080	2007 Feb 01 - 2007 Mar 04	Y	12 hours	PM10, PM10-100	5.56E-03	25	16	N/A	N/A	N/A	1.4E-01	7.33E+00
Takeuchi et al. (2012)	Tokushima, Japan	U	34.067	134.500	2011 Dec	N	3 hours	PM0.21-7.8	3.5E-01	12	7	N/A	N/A	N/A	4.45E-01	6.18E+00
Shirahata (2012)	Lake Toya, Hokkaido, Japan	R	42.567	140.825	2011 Jul to 2012 Feb	Y	1/0.5 months	N/A	1E-02	4	0	N/A	N/A	N/A	N/A	N/A
Yao et al. (2015)	Jinan, China	U	36.667	117.050	2013 Jan 12 to 2013 Feb 10	Y	3 times a day	PM2.5	1.52E-01	67	67	1.62E+00	1.11E+00	2.55E-01	1.47E+00	7.21E+00
	Kumamoto, Japan	U	32.800	130.700	2012 Nov 08 to 2013 Dec 08	N	72/96 hours	PM0.43, PM2.1-3.3, PM11-100	3.27E-03	7	7	4.34E-02	2.31E-02	1.98E-02	3.96E-02	9.25E-02
C. Wang et al. (2017)	Changsha, China	U	28.180	112.947	2016 Jul 20 to 2016 Jul 31	N	Daily	> 9.0, 5.8~9.0,	N/A	5	5	1.82E+01	2.6E+00	1.49E+01	1.84E+01	2.21E+01

								4.7~5.8, 3.3~4.7, 2.1~3.3, 1.1~2.1, 0.7~1.1, 0.4~0.7, and < 0.4 μm							
H. Zhu et al. (2021)	Beijing, China	U	39.904	116.407	2017 Mar 31 to 2017 Apr 06	N	Daily	PM2.5	9.09E-01	7	7	3.74E+01	2.29E+01	1.15E+01	3.15E+01	7.83E+01
	Tianjin, China	U	39.085	117.199	2017 Mar 28 to 2017 Apr 06	N	Daily	PM2.5	9.09E-01	7	7	2.65E+01	8.79E+00	1.82E+01	2.52E+01	4.2E+01
	Zhengzhou, China	U	34.747	113.625	2017 Mar 30 to 2017 Apr 05	N	Daily	PM2.5	9.09E-01	7	7	2.04E+01	1.34E+01	1.72E+00	2.27E+01	3.46E+01
	Jinan, China	U	36.652	117.120	2017 Mar 30 to 2017 Apr 05	N	Daily	PM2.5	9.09E-01	7	7	2.37E+01	1.07E+01	1.29E+01	2.03E+01	4.16E+01
	Baoding, China	U	38.874	115.465	2017 Mar 30 to 2017 Apr 06	N	Daily	PM2.5	9.09E-01	7	7	5.21E+01	2.1E+01	3.5E+01	4.41E+01	9.44E+01
	Shijazhuang, China	U	38.043	114.514	2017 Mar 31 to 2017 Apr 06	N	Daily	PM2.5	9.09E-01	7	7	2.79E+01	1.99E+01	8.74E+00	1.5E+01	5.49E+01
	TBH-region overall	U	N/A	N/A	2017 Mar 28 to 2017 Apr 06	N	Daily	PM2.5	9.09E-01	42	42	3.16E+01	1.92E+01	1.72E+00	2.87E+01	9.44E+01
Zheng et al. (2022)	Longgang, Shenzhen, China	U	22.592587	114.479546	2020 Oct to 2021 Sept	N	7 Daily samples a month	PM2.5	7.94E-03	84	80	N/A	N/A	N/A	5.8E-02	4.11E-01
	Nanshan, Shenzhen, China	U	22.531061	113.932433	2020 Oct to 2021 Sept	N	7 Daily samples a month	PM2.5	7.94E-03	84	80	N/A	N/A	N/A	4.6E-02	1.14E+00
	Yantian, Shenzhen, China	U	22.573762	114.266488	2020 Oct to 2021 Sept	N	7 Daily samples a month	PM2.5	7.94E-03	84	80	N/A	N/A	N/A	5.1E-02	3.28E-01

	Shenzhen overall	U	N/A	N/A	2020 Oct to 2021 Sept	N	7 Daily samples a month at each site	PM2.5	7.94E-03	252	240	N/A	N/A	N/A	4.9E-02	1.14E+00
Jiang et al. (2021)	Open-ocean	B	N/A	N/A	2015 Nov 08 to 2016 Apr 10	N	24-72 hours	N/A	6.17E-06 - 1.85E-05	22	22	7.7E-02	8.49E-02	5E-03	3.4E-02	3.11E-01
	Near-coast	B	N/A	N/A	2015 Nov 07 to 2016 Apr 06	N	24-72 hours	N/A	6.17E-06 - 1.85E-05	20	20	1.34E-01	1.43E-01	1E-03	1E-01	5.74E-01
	Antarctica	B	N/A	N/A	2015 Dec 15 to 2016 Feb 04	N	24-72 hours/ 7 days	N/A	6.17E-06 - 1.85E-05	34	34	1.63E-01	8.25E-02	7E-02	1.34E-01	4.23E-01
	Overall	B	N/A	N/A	2015 Nov 07 to 2016 Apr 10	N	24-72 hours/ 7 days	N/A	6.17E-06 - 1.85E-05	76	76	1.3E-01	1.07E-01	1E-03	1.02E-01	5.74E-01

Notes:

Site types: Urban (U), Rural (R), Background (B).

For statistical metrics, the choice of showing 3 significant figures is for display purposes only and has no implications for measurement precision.

For Yamada et al. (2009, 2012), the mean, the standard deviation, and the range are obtained from the main text of Yamada et al. (2012). The detection limit is estimated by 160 ng/L × 0.015 L/ (0.1 m^3/min × 12 hr × 60 min/hr) / 0.25 filter fraction = 0.0133 ng/m3. The individual measurements were originally plotted in Yamada et al. (2009)'s Figure 6 and Yamada et al. (2012)'s Figure 1. We obtained the 131 measurements of perchlorate atmospheric concentration via email communication with Professor Etsu Yamada and use the data to compute the median. They used ion chromatography and a concentrator column for their sample analysis.

For Handa et al. (2010), detection limit and maximum are obtained from the main text. The individual measurements were originally plotted in Handa et al. (2010)'s Figure 2. We obtained the 60 measurements of perchlorate atmospheric

concentration via email communication with Professor Takemitsu Arakaki and use the data to compute the median. They used ion chromatography for their sample analysis.

For Y. Shi et al. (2011), the individual measurements are obtained from their Table 2. We combine the $PM_{10\text{-}100}$ and PM_{10} data to estimate the statistics for perchlorate in PM_{100}. The detection limit is estimated by 20 ng/L × 0.02 L/ (0.1 m^3/min × 12 hr × 60 min/hr) = 0.00556 ng/m^3. Y. Shi et al. (2011) suggested the measurements in the period of 2007 Feb 17 to 2007 Feb 22 and on 2007 Mar 03 are under the influence of spring-festival fireworks and firecrackers. The measurements from these 7 days are excluded from our analysis. They used ion chromatography coupling with an electrospray tandem mass spectrometer (IC-ESI-MS) for their analysis

For Takeuchi et al. (2012), the individual measurements were originally plotted in their Figure 7. We obtained the 12 measurements of perchlorate atmospheric concentration via email communication with Professor Masaki Takeuchi and use the data to compute the median. They estimated the mean and standard deviation by substituting the seven under-detection-limit observations with 0 ng m^{-3}. They reported an average and standard deviation of 1.01 ng m^{-3} and 1.75 ng m^{-3}, respectively. They used ion chromatography and concentrator columns for their sample analysis.

For Shirahata (2012), only the measurements from November to February are considered because they reported that daily fireworks take place near Lake Toya from late April to late October every year. All the reported non-fireworks observations do not contain detectable levels of perchlorate. They used ion chromatography and a concentrator column for their sample analysis.

For Yao et al. (2015)'s Jinan observations, we extract the measured values from their Figure 2. The Spring-Festival-Eve observations on 2013 Feb 09 and 2013 Feb 10 are excluded from our analysis because of the large influence of fireworks. The detection limit for Jinan observations is 20 ng/L × 0.02 L / (0.00733 m3/min × 6 hr × 60 min/hr) = 0.152 ng m^{-3}. For their Kumamoto observations, we combine measurements from all aerosol-size bins to estimate perchlorate concentration in PM_{100}. The mean is obtained from adding the averages reported from the main text while other statistics are computed using the extracted data. The detection limit for Kumamoto observations is estimated by 20 ng/L × 0.02 L / (0.0283 m3/min × 72 hr × 60 min/hr)=0.00327 ng m^{-3}. They used ion chromatography coupling with an electrospray tandem mass spectrometer (IC-ESI-MS/MS) for their analysis. We contacted the corresponding author of the paper to ask for more information but have not received any response.

For C. Wang et al. (2017), we extract their measured values from their Figure 3. The measurements for different aerosol-size bins are combined to get the total perchlorate concentration. They used ion chromatography for their sample analysis. We contacted the corresponding author of the paper to ask for more information but have not received any response.

For H. Zhu et al. (2021), we extract their measured values from their Figure 1. They did not specify the exact location of their site. We use the latitude and longitude of the center of the cities that they studied as the site location because they stated their sites are located in the "central region" of these cities. They used ion chromatography for their sample analysis. We contacted the corresponding authors of the paper to ask for more information but have not received any response.

For Zheng et al. (2022), we obtain the statistics of the measurements from their Table 1. The detection limit is 100 ng/L × 0.01 L/ (0.35 m^3/min × 24 hr × 60 min/hr)/0.25 filter fraction = 0.00794 ng m^{-3}. They used high-performance liquid chromatography coupling with a Q-Trap tandem mass spectrometer in negative-electrospray-ionization-and-multi-reaction-monitoring mode for their analysis.

For Jiang et al. (2021), we obtain their measurements from their Table S1. We group their measurements into three categories (open-ocean: reported location ≥200km away from the coast; near-coast: reported location <200km away from the coast; and Antarctic: observations in Antarctica). They used ion chromatography coupled with an electrospray tandem mass spectrometer (IC-ESI-MS/MS) for their analysis. G. Shi et al. (2018) was cited for the filter-extraction method, where 100 ml of Milli-Q water was used to extract solution ions from the filters. The lower detection limit is 0.2 ng/L × 0.1 L / (1 m^3/ min ×72 hr × 60 min /hr)/0.75 filter fraction =6.17×10^{-6} ng m^{-3}. The upper detection limit is 2 ng/L × 0.1 L / (1 m^3/ min ×24 hr × 60 min /hr)/0.75 filter fraction =1.85×10^{-5} ng m^{-3}.

Gan et al. (2014), Vella et al. (2015), and Li et al. (2016, 2018) reported the mass mixing ratios of perchlorate (i.e., mass of ClO_4^- per unit mass of sample) in outdoor-dust samples collected from China and Malta. We did not include these observations in our analysis because there is no trivial way to convert mass mixing ratios to atmospheric mass concentration (i.e., in mass of ClO_4^- per unit volume of air) without assuming a certain mass concentration, size distribution, and/or deposition rate of outdoor dust, which are highly uncertain.

Table S3. Summary of observations of perchlorate during non-fireworks periods in deposition samples reported in different studies

Study	Geographic location	Site type	Lat (°)	Long (°)	Sampling period	Study reported clear fireworks influence? (Y/N)	Sampling Freq.	# Obs	# Detect	Long-term mean dep flux (g km^{-2} yr^{-1})	Long-term mean dep conc (µg L^{-1})	Long-term mean precipitation or accumulation rate (mm day^{-1})
Munster et al. (2009)	Coram, NY, USA	T	40.880434	-73.010131	2005 Dec to 2007 Mar	Y	Monthly	15	15	3.93E+02	3.06E-01	4.24E+00
	East Hampton, NY, USA	T	40.954703	-72.206717	2005 Dec to 2007 Jan	Y	Monthly	12	12	5.58E+01	5.61E-02	3.43E+00
	Hauppauge, NY, USA	T	40.807406	-73.251751	2005 Dec to 2007 Jun	Y	Monthly	18	15	1.37E+02	8.24E-02	4.33E+00
	Huntington, NY, USA	T	40.86985	-73.418043	2005 Dec to 2007 Jun	Y	Monthly	17	15	8.76E+01	6.51E-02	4.48E+00
	Oakdale, NY, USA	T	40.748627	-73.136915	2005 Dec to 2007 Jun	Y	Monthly	18	18	1.56E+02	1.04E-01	3.98E+00
	Stony Brook, NY, USA	T	40.915318	-73.125848	2006 Jan to 2007 Jun	Y	Monthly	16	16	3.86E+02	1.70E-01	4.38E+00
Andraski et al. (2014)	Amargosa Desert, NV, USA	T	36.765	-116.693	2005 Aug to 2011 Aug	N	~1-4 months	22	22	3.43E+01	6.08E-01	2.42E-01
Rajagopalan et al. (2009)	Juneau, AK, USA	W	58.514	-134.784	2004 Oct to 2007 Oct	N	Weekly	72	N/A	6.79E+00	1.14E-02	1.63E+00
	Coconino, AZ, USA	W	36.059	-112.184	2004 Oct to 2007 Oct	N	Weekly	70	N/A	3.35E+00	1.44E-02	6.36E-01
	Cochise, AZ, USA	W	32.010	-109.389	2004 Oct to 2007 Oct	N	Weekly	55	N/A	3.46E+00	1.48E-02	6.43E-01

	Tuolumne, CA, USA	W	37.796	-119.858	2006 Oct to 2007 Oct	N	Weekly	13	N/A	2.68E+00	8.38E-03	8.75E-01
	Garfield, CO, USA	W	39.426	-107.380	2004 Oct to 2007 Oct	N	Weekly	102	N/A	8.26E+00	1.59E-02	1.42E+00
	Brevard, FL, USA	W	28.543	-80.644	2004 Oct to 2007 Oct	N	Weekly	106	N/A	7.26E+00	9.62E-03	2.07E+00
	Butte, ID, USA	W	43.461	-113.555	2004 Oct to 2007 Oct	N	Weekly	51	N/A	2.52E+00	1.53E-02	4.53E-01
	Riley, KS, USA	W	39.102	-96.609	2004 Oct to 2007 Oct	N	Weekly	91	N/A	1.16E+01	1.65E-02	1.93E+00
	Somerset, MD, USA	W	37.992	-76.034	2004 Oct to 2007 Oct	N	Weekly	88	N/A	7.42E+00	1E-02	2.02E+00
	Piscataquis, ME, USA	W	45.489	-69.665	2006 Oct to 2007 Oct	N	Weekly	34	N/A	8.76E+00	1.13E-02	2.11E+00
	Itasca, MN, USA	W	47.531	-93.469	2006 Oct to 2007 Oct	N	Weekly	31	N/A	8.04E+00	1.43E-02	1.54E+00
	St. Louis, MO, USA	W	38.519	-90.565	2006 Oct to 2007 Oct	N	Weekly	28	N/A	6.55E+00	1.11E-02	1.62E+00
	Yalobusha, MS, USA	W	34.002	-89.799	2006 Oct to 2007 Oct	N	Weekly	31	N/A	1.12E+01	1.17E-02	2.61E+00
	Big Horn, MT, USA	W	45.570	-107.438	2004 Oct to 2007 Oct	N	Weekly	73	N/A	5.21E+00	1.96E-02	7.3E-01
	Rowan, NC, USA	W	35.697	-80.623	2006 Oct to 2007 Oct	N	Weekly	26	N/A	6.42E+00	1.27E-02	1.38E+00
	Lincoln, NE, USA	W	41.059	-100.746	2004 Oct to 2007 Oct	N	Weekly	62	N/A	1.01E+01	2.19E-02	1.26E+00
	Los Alamos, NM, USA	W	35.779	-106.266	2004 Oct to 2007 Oct	N	Weekly	69	N/A	4.18E+00	1.64E-02	6.97E-01
	White Pine, NV, USA	W	39.005	-114.217	2004 Oct to 2007 Oct	N	Weekly	62	N/A	4.01E+00	2.19E-02	5E-01
	Butler, OH, USA	W	39.531	-84.724	2006 Oct to 2007 Oct	N	Weekly	33	N/A	7.15E+00	1.25E-02	1.56E+00
	Alfalfa, OK, USA	W	36.786	-98.180	2004 Oct to 2007 Oct	N	Weekly	80	N/A	8.32E+00	1.54E-02	1.48E+00
	Benton, OR, USA	W	44.386	-123.615	2006 Oct to 2007 Oct	N	Weekly	31	N/A	7.39E+00	1.09E-02	1.85E+00

	Rio Grande, Puerto Rico	W	18.321	-65.820	2004 Oct to 2007 Oct	N	Weekly	117	N/A	1.36E+01	7.26E-03	5.13E+00
	Bailey, TX, USA	W	33.956	-102.776	2004 Oct to 2007 Oct	N	Weekly	56	N/A	5.65E+00	1.57E-02	9.87E-01
	Brewster, TX, USA	W	29.302	-103.178	2004 Oct to 2007 Oct	N	Weekly	52	N/A	2.73E+00	1.46E-02	5.11E-01
	Garfield, UT, USA	W	37.619	-112.173	2004 Oct to 2007 Oct	N	Weekly	66	N/A	3.82E+00	1.48E-02	7.05E-01
	Whitman, WA, USA	W	46.761	-117.185	2004 Oct to 2007 Oct	N	Weekly	79	N/A	4.70E+00	1.46E-02	8.81E-01
	Overall	W	N/A	N/A	2004 Oct to 2007 Oct	N	Weekly	1578	N/A	8.61E+02	1.4E-02	1.29E+00
Yamada et al. (2009, 2012)	Kyoto, Japan	W	35.050	135.780	2007 Aug to 2009 Oct	N	Daily	36	29	1.79E+04	5.11E-01	3.94E+00
Lin et al. (2019)	Guangzhou, China	W	23.166	113.365	2016 Oct to 2017 Sept	Y	Continuous for a year	80	69	4.93E+01	1.60E+01	4.33E+00
Van Stempvoort et al. (2020)	Cedar Creek, Southern Ontario, Canada	W	43.084	-80.736	2017 Aug to 2019 Jul	N, see notes	2-4 weeks	43	43	3.74E+01	6.88E-02	1.96E+00
	Nissouri Creek, Southern Ontario, Canada	W	43.115	-80.969	2017 Aug to 2019 Jul	N, see notes	2-4 weeks	36	36	1.32E+01	4.23E-02	2.42E+00
Jiang et al. (2020)	32A snow pit, Antarctica	I	-69.790	76.490	Post 1980	N	N/A	N/A	N/A	1.80E+01	4.23E-02	4.02E-01
	32C snow pit, Antarctica	I	-76.420	77.030	Post 1980	N	N/A	N/A	N/A	5.25E+00	4.23E-02	2.27E-01
Jiang et al. (2016)	Dome A, Antarctica	I	-80.367	77.367	Post 1980	N	N/A	N/A	N/A	5.01E+00	4.23E-02	6.3E-02
	South Pole	I	-90.000	0.000	Post 1980	N	N/A	N/A	N/A	9.60E+00	4.23E-02	2.3E-01
Crawford et al. (2017)	WAIS Divide, Antarctica	I	-79.467	-112.085	Post 1980	N	N/A	N/A	N/A	6.10E-01	4.23E-02	5.48E-01
Cole-Dai et al. (2018)	Summit, Greenland	I	73.600	-38.500	Post 1980	N	N/A	N/A	N/A	4.50E-01	4.23E-02	6.19E-01
	TUNU, Greenland	I	78.100	-34.000	Post 1980	N	N/A	N/A	N/A	1.15E+00	4.23E-02	3.42E-01

	Basin 4, Greenland	I	62.300	-46.300	Post 1980	N	N/A	N/A	N/A	1.69E+00	4.23E-02	1.13E+00
Furdui & Tomassini (2010)	Devon Ice Cap, Canada	I	75.333	-82.667	Post 1980	N	N/A	N/A	N/A	1.11E+00	4.23E-02	6.6E-01
Furdui et al. (2018)	Agassiz Ice Cap, Canada	I	80.700	-73.100	Post 1980	N	N/A	N/A	N/A	2.99E+00	4.23E-02	2.74E-01
Rao et al. (2012)	Eclipse Icefield, Canada	I	60.510	-139.470	Post 1980	N	N/A	N/A	N/A	1.40E+00	4.23E-02	3.56E+00
	Upper Fremont Glacier, USA	I	43.117	-109.617	Post 1980	N	N/A	N/A	N/A	4.80E+00	4.23E-02	2.08E+00
Du et al. (2019)	Tienshan, China	I	43.055	94.323	Post 1980	N	N/A	N/A	N/A	3.93E+02	4.23E-02	7.12E-01

Notes:

Sample types: Total deposition: T; Wet deposition: W; Ice-core/snow-pit: I

Long-term mean precipitation or accumulation rate: At sites that collected wet-deposition and total-deposition samples, it represents the long-term mean precipitation rate (unit: mm per day). At ice-core/snow-pit sites, it represents the long-term mean accumulation rate (unit: mm water equivalent per day).

Many studies that analyzed perchlorate concentration in deposition samples did not report the corresponding perchlorate deposition flux, which is valuable for model evaluation. We use MERRA-2 precipitation data to estimate the perchlorate deposition flux when precipitation statistics were not reported.

For Munster et al. (2009), we obtain their measurements from the appendix table of the first author's PhD dissertation (Munster, 2008). After removing duplicates, we obtain the perchlorate measurements for 107 samples. This number is very close to the number stated in Munster et al. (2009) ("a total of 108 samples"). Munster et al. (2009)'s samples were collected using all-weather precipitation gauges, which were not covered during dry periods, and thus are classified as total-deposition samples. The site locations were shown in Figure 1 of Munster et al. (2009), but the paper did not specify the exact latitudes and longitudes. We obtained the latitude and longitude of each site via email communication with Dr. Jennie Munster. We

exclude July measurements to minimize the influence of Fourth-of-July fireworks displays. Although Munster (2008)'s appendix reports the volume of precipitation samples, several values are invalid (e.g., > volume of precipitation gauge). Therefore, we estimate the precipitation rate at each site using the nearest-grid value from MERRA-2 total precipitation data. Munster et al. (2009) used sequential ion chromatography-mass spectroscopy/mass spectroscopy (IC-MS/MS) to analyze the perchlorate content in their precipitation samples with a detection limit of 0.005 μg L^{-1}. For under-detection-limit measurements, we substitute them by 0.005 μg L^{-1} and 0 μg L^{-1} to compute the upper-bound and lower-bound estimate of long-term mean deposition concentration and flux. The two estimates of long-term perchlorate deposition flux differ by about 1%. We show the upper-bound estimate in the table, but the choice does not affect the conclusion from our analysis.

For Andraski et al. (2014), we obtain the long-term mean perchlorate deposition flux, perchlorate concentration, and precipitation rate (=535 mm/2207 days) from their main text. Both rainfall and dust were collected by their field instruments, so their samples are classified as total deposition. Andraski et al. (2014) used ion chromatography-mass spectroscopy/mass spectroscopy (IC-MS/MS) to analyze the perchlorate content in their precipitation samples. They mentioned that their method detection limit is 0.01 μmol L^{-1} (i.e., 0.9945 μg L^{-1}), which seems to be higher than at least half of their measurements reported. We suspect that it is a typo.

For Rajagopalan et al. (2009), we obtain the long-term mean perchlorate deposition flux, perchlorate concentration, and precipitation rate (reported average flux/ reported average concentration) from their Table S1. Rajagopalan et al. (2009) used sequential ion chromatography-mass spectroscopy/mass spectroscopy (IC-MS/MS) to analyze the perchlorate content in their precipitation samples with a limit of quantification of 5 ng L^{-1}.

For Yamada et al. (2009, 2012), we obtain their measurements from Table 1 of Yamada et al. (2009) and Table 1 of Yamada et al. (2012). They used ion chromatography and a concentrator column for analyzing perchlorate content in wet-deposition samples. The detection limit is 0.16 μg L^{-1}. We estimate the monthly precipitation rate at the Kyoto site using the nearest-grid value from MERRA-2 total precipitation data. We compute the monthly average perchlorate concentration from the daily measurements. For under-detection-limit measurements, we substitute them by 0.16 μg L^{-1} and 0 μg L^{-1} to compute the upper-bound and lower-bound estimate of long-term mean deposition concentration and flux. The two estimates of long-term perchlorate deposition flux differ by about 5%. We show the upper-bound estimate in the table, but the choice does not affect the conclusion from our analysis.

For Lin et al. (2019), only the statistics (quantiles and outliers) of perchlorate measurements were shown in their Figure 3. We obtained the 81 perchlorate measurements via email communication with Professor Huashou Li and Dr. Xiaoyang Lin. They used ion chromatography for their perchlorate analysis with a detection limit of 1 ppb (1 μg L^{-1}). The 2017-02-08 sample is

not considered in the analysis because of the potential large influence of spring-festival fireworks. We estimate the monthly precipitation rate at the Guangzhou site using the nearest-grid value from MERRA-2 total precipitation data. We compute the monthly average perchlorate concentration using the 80 perchlorate measurements. For under-detection-limit measurements, we substitute them by 1 μg L^{-1} and 0 μg L^{-1} to compute the upper-bound and lower-bound estimate of long-term mean deposition concentration and flux. The two estimates of long-term perchlorate deposition flux differ by less than 2%. We show the upper-bound estimate in the table, but the choice does not affect the conclusion from our analysis.

For Van Stempvoort et al. (2020), we obtain the long-term mean perchlorate concentration and deposition flux from their Table S3 and Text S6. The long-term mean precipitation rate at each site is inferred by dividing perchlorate deposition flux by perchlorate concentration. They used ion chromatography coupled with tandem mass spectrometry for their sample analysis with a detection limit of 1 ng L^{-1}. The paper mentioned the potential fireworks influence on perchlorate concentration in samples collected around Victoria Day (2017 May 22, 2018 May 21, 2019 May 20) and Canada Day (July 1 every year). We try to re-estimate the long-term deposition flux at each site using non-fireworks-influenced samples and MERRA-2 total precipitation data, similar to the method we use for the other sites. We find higher perchlorate fluxes (59.7 g km^{-2} $year^{-1}$ at Cedar Creek and 47.2 g km^{-2} $year^{-1}$ at Nissouri Creek) after removing the samples that were potentially influenced by fireworks displays. We contacted the corresponding author of the paper to ask for more information but have not received any response.

For ice-core/snow-pit sites, we obtain the post-1980s long-term mean perchlorate concentration, deposition flux, and accumulation rate at each site from Jiang et al. (2020)'s Table 1.

We found that 7 other studies (Barron et al., 2006; Dasgupta et al., 2005; Kannan et al., 2009; Pace & Vella, 2019; Qin et al., 2014; Sijimol et al., 2016; Ye et al., 2013) had reported measurements of perchlorate concentration in deposition samples. However, they are not included in our analysis for long-term deposition flux because their sampling periods are shorter than a year.

Table S4. Model bias in long-term perchlorate deposition flux

Sample type	Group	Observation (g km-2 year-1)	Model (g km-2 year-1)	Model abs bias (g km-2 year-1)	Model rel bias (%)	Obs/Model ratio	Reference
Summary							
W	Median of all US NADP sites (# sites = 26)	6.67E+00	4.20E+00	-2.47E+00	-3.7E+01	1.59E+00	Refer to individual records below
W&T	Median of all NH non-ice-core-snow-pit sites (# sites = 37)	8.04E+00	4.60E+00	-3.44E+00	-4.28E+01	1.75E+00	
I	Median of all NH ice-core-snow-pit sites (# sites = 8)	1.28E+00	9.63E-01	-3.12E-01	-2.45E+01	1.32E+00	
I	Median of all Antarctic sites (# sites = 5)	9.60E+00	3.34E-01	-9.27E+00	-9.65E+01	2.88E+01	
W,T&I	Median of all site (# sites = 50)	7.21E+00	3.69E+00	-3.52E+00	-4.88E+01	1.95E+00	

Comparison at individual sites

Sample type	Location	Site Name	Lat	Lon	Observation (g km-2 year-1)	Model (g km-2 year-1)	Model absolute bias (g km-2 year-1)	Model relative bias (%)	Obs/Model ratio	Reference
T	Coram, NY, USA	Coram	40.869	-73.001	3.93E+02	5.83E+00	-3.88E+02	-9.85E+01	6.75E+01	Munster et al. (2009)
T	East Hampton, NY, USA	East Hampton	40.963	-72.185	5.58E+01	4.96E+00	-5.08E+01	-8.96E+01	9.64E+00	
T	Hauppauge, NY, USA	Hauppauge	40.826	-73.203	1.37E+02	5.83E+00	-1.31E+02	-9.58E+01	2.36E+01	Munster et al. (2009)
T	Huntington, NY, USA	Huntington	40.868	-73.426	8.76E+01	5.83E+00	-8.18E+01	-9.34E+01	1.5E+01	Munster et al. (2009)
T	Oakdale, NY, USA	Oakdale	40.744	-73.139	1.56E+02	5.83E+00	-1.51E+02	-9.63E+01	2.68E+01	Munster et al. (2009)
T	Stony Brook, NY, USA	Stony Brook	40.926	-73.141	3.86E+02	5.83E+00	-3.80E+02	-9.85E+01	6.62E+01	Munster et al. (2009)

T	Amargosa Desert, NV, USA	Weather station of USGS Amargosa Desert Research Site	36.765	-116.693	3.43E+01	2.47E+00	-3.18E+01	-9.28E+01	1.39E+01	Andraski et al. (2014)
W	Juneau, AK, USA	NADP AK02	58.514	-134.784	6.79E+00	3.43E+00	-3.36E+00	-4.95E+01	1.98E+00	Rajagopalan et al. (2009)
W	Coconino, AZ, USA	NADP AZ03	36.059	-112.184	3.35E+00	2.90E+00	-4.49E-01	-1.34E+01	1.15E+00	
W	Cochise, AZ, USA	NADP AZ98	32.010	-109.389	3.46E+00	2.42E+00	-1.04E+00	-3E+01	1.43E+00	
W	Tuolumne, CA, USA	NADP CA99	37.796	-119.858	2.68E+00	3.14E+00	4.62E-01	1.72E+01	8.53E-01	
W	Garfield, CO, USA	NADP CO92	39.426	-107.380	8.26E+00	4.06E+00	-4.20E+00	-5.09E+01	2.04E+00	
W	Brevard, FL, USA	NADP FL99	28.543	-80.644	7.26E+00	6.85E+00	-4.18E-01	-5.75E+00	1.06E+00	
W	Butte, ID, USA	NADP ID03	43.461	-113.555	2.52E+00	2.66E+00	1.37E-01	5.45E+00	9.48E-01	
W	Riley, KS, USA	NADP KS31	39.102	-96.609	1.16E+01	6.74E+00	-4.86E+00	-4.19E+01	1.72E+00	
W	Somerset, MD, USA	NADP MD15	37.992	-76.034	7.42E+00	5.83E+00	-1.59E+00	-2.14E+01	1.27E+00	
W	Piscataquis, ME, USA	NADP ME09	45.489	-69.665	8.76E+00	4.67E+00	-4.09E+00	-4.67E+01	1.88E+00	
W	Itasca, MN, USA	NADP MN16	47.531	-93.469	8.04E+00	4.45E+00	-3.58E+00	-4.46E+01	1.8E+00	
W	St. Louis, MO, USA	NADP MO43	38.519	-90.565	6.55E+00	7.93E+00	1.38E+00	2.11E+01	8.26E-01	
W	Yalobusha, MS, USA	NADP MS30	34.002	-89.799	1.12E+01	8.49E+00	-2.66E+00	-2.38E+01	1.31E+00	
W	Big Horn, MT, USA	NADP MT00	45.570	-107.438	5.21E+00	3.01E+00	-2.21E+00	-4.23E+01	1.73E+00	
W	Rowan, NC, USA	NADP NC34	35.697	-80.623	6.42E+00	6.34E+00	-7.67E-02	-1.19E+00	1.01E+00	
W	Lincoln, NE, USA	NADP NE99	41.059	-100.746	1.01E+01	4.60E+00	-5.49E+00	-5.44E+01	2.19E+00	
W	Los Alamos, NM, USA	NADP NM07	35.779	-106.266	4.18E+00	2.58E+00	-1.59E+00	-3.81E+01	1.62E+00	
W	White Pine, NV, USA	NADP NV05	39.005	-114.217	4.01E+00	2.25E+00	-1.75E+00	-4.38E+01	1.78E+00	
W	Butler, OH, USA	NADP OH09	39.531	-84.724	7.15E+00	7.77E+00	6.16E-01	8.62E+00	9.21E-01	
W	Alfalfa, OK, USA	NADP OK00	36.786	-98.180	8.32E+00	4.35E+00	-3.97E+00	-4.77E+01	1.91E+00	

W	Benton, OR, USA	NADP OR02	44.386	-123.615	7.39E+00	4.67E+00	-2.72E+00	-3.68E+01	1.58E+00	
W	Rio Grande, Puerto Rico	NADP PR20	18.321	-65.820	1.36E+01	4.45E+00	-9.16E+00	-6.73E+01	3.06E+00	
W	Bailey, TX, USA	NADP TX02	33.956	-102.776	5.65E+00	2.58E+00	-3.07E+00	-5.43E+01	2.19E+00	
W	Brewster, TX, USA	NADP TX04	29.302	-103.178	2.73E+00	2.36E+00	-3.71E-01	-1.36E+01	1.16E+00	
W	Garfield, UT, USA	NADP UT99	37.619	-112.173	3.82E+00	2.90E+00	-9.17E-01	-2.4E+01	1.32E+00	
W	Whitman, WA, USA	NADP WA24	46.761	-117.185	4.70E+00	3.76E+00	-9.45E-01	-2.01E+01	1.25E+00	
W	Kyoto, Japan	Kyoto Institute of Technology, Building No.12	35.050	135.780	8.61E+02	5.59E+00	-8.55E+02	-9.94E+01	1.54E+02	Yamada et al. (2009, 2012)
W	Guangzhou, China	South China Agricultural University	23.166	113.365	1.79E+04	3.62E+00	-1.79E+04	-1E+02	4.93E+03	Lin et al. (2019)
W	Cedar Creek, Southern Ontario, Canada	Cedar Creek Sub Basin	43.084	-80.736	4.93E+01	5.75E+00	-4.35E+01	-8.83E+01	8.57E+00	Van Stempvoort et al. (2020)
W	Nissouri Creek, Southern Ontario, Canada	Nissouri Creek Sub Basin	43.115	-80.969	3.74E+01	5.75E+00	-3.16E+01	-8.46E+01	6.50E+00	
I	32A snow pit, Antarctica	32A snow pit	-69.790	76.490	1.32E+01	5.02E-01	-1.27E+01	-9.62E+01	2.63E+01	Jiang et al. (2020)
I	32C snow pit, Antarctica	32C snow pit	-76.420	77.030	1.80E+01	3.16E-01	-1.77E+01	-9.82E+01	5.71E+01	
I	Dome A, Antarctica	Dome A	-80.367	77.367	5.25E+00	1.91E-01	-5.06E+00	-9.64E+01	2.74E+01	Jiang et al. (2016)
I	South Pole	South Pole	-90.000	0.000	5.01E+00	3.34E-01	-4.68E+00	-9.33E+01	1.5E+01	
I	WAIS Divide, Antarctica	WAIS Divide	-79.467	-112.085	9.60E+00	4.66E-01	-9.13E+00	-9.51E+01	2.06E+01	Crawford et al. (2017)
I	Summit, Greenland	Summit	73.600	-38.500	6.10E-01	4.92E-01	-1.18E-01	-1.94E+01	1.24E+00	Cole-Dai et al. (2018)
I	TUNU, Greenland	TUNU	78.100	-34.000	4.50E-01	2.93E-01	-1.57E-01	-3.5E+01	1.54E+00	
I	Basin 4, Greenland	Basin 4	62.300	-46.300	1.15E+00	2.26E+00	1.11E+00	9.61E+01	5.1E-01	Cole-Dai et al. (2018)
I	Devon Ice Cap, Canada	Devon Ice Cap	75.333	-82.667	1.69E+00	6.15E-01	-1.08E+00	-6.36E+01	2.75E+00	Furdui & Tomassini (2010)
I	Agassiz Ice Cap, Canada	Agassiz Ice Cap	80.700	-73.100	1.11E+00	3.95E-01	-7.15E-01	-6.44E+01	2.81E+00	Furdui et al. (2018)
I	Eclipse Icefield, Canada	Eclipse Icefield	60.510	-139.470	2.99E+00	1.98E+00	-1.01E+00	-3.39E+01	1.51E+00	Rao et al.

I	Upper Fremont Glacier, USA	Upper Fremont Glacier, USA	43.117	-109.617	1.40E+00	4.06E+00	2.66E+00	1.9E+02	3.45E-01	(2012)
I	Tienshan, China	Tienshan	43.055	94.323	4.80E+00	1.31E+00	-3.49E+00	-7.27E+01	3.66E+00	Du et al. (2019)

Notes:

Sample types: Total deposition: T; Wet deposition: W; Ice-core/snow-pit: I

Model absolute bias = modeled value – observed value
Model relative bias = (modeled value – observed value)/observed value×100%

Table S5. Observed $\Delta^{17}O(ClO_4^-)$ in 149 environmental samples reported in different studies

Study	Sample identification	Geographic location	Sample type	$\Delta^{17}O(ClO_4^-)$ (‰)
Jackson et al. (2010)	Zabriskie	Death Valley, USA	Soil	+18.4
Estrada et al. (2021)	N/A	McMurdo Dry Valleys, Antarctica	Soil	+14.0
Jackson et al. (2016)	MDV single dry soil sample	McMurdo Dry Valleys, Antarctica	Soil	+12.8
Jackson et al. (2010)	Confidence Hills 2	Death Valley, USA	Soil	+12.8
Jackson et al. (2021)	Confidence Hills (6H)	Death Valley, USA	Soil	+12.3
Estrada et al. (2021)	N/A	McMurdo Dry Valleys, Antarctica	Soil	+12.2
Jackson et al. (2010)	Saratoga Hills	Death Valley, USA	Soil	+10.9
Böhlke et al. (2005)	N/A	Atacama Desert, Chile	Soil	+10.55
Böhlke et al. (2005)	N/A	Atacama Desert, Chile	Soil	+10.55
Böhlke et al. (2009)	DL4d	Long Island, NY, USA	Groundwater	+10.2
Böhlke et al. (2005)	N/A	Atacama Desert, Chile	Soil	+9.68
Bao & Gu (2004)	AT24-1-CsClO4	Atacama Desert, Chile	Soil	+9.6
Bao & Gu (2004)	AT74-1-CsClO4	Atacama Desert, Chile	Soil	+9.6
Sturchio et al. (2006)	ORNL-5	Atacama Desert, Chile	Nitrate deposit	+9.57
Jackson et al. (2010)	GJ01	Atacama Desert, Chile	Soil	+9.4
Böhlke et al. (2009)	NP1	Long Island, NY, USA	Groundwater	+9.4
Böhlke et al. (2005)	N/A	Atacama Desert, Chile	Soil	+9.37
Jackson et al. (2010)	UIC-25	Chile	Groundwater	+9.3
Böhlke et al. (2005)	N/A	Atacama Desert, Chile	Soil	+9.23
Böhlke et al. (2005)	N/A	Atacama Desert, Chile	Soil	+9.23
Jackson et al. (2010)	P2	Atacama Desert, Chile	Soil	+9.2
Böhlke et al. (2005)	N/A	Atacama Desert, Chile	Soil	+9.06
Böhlke et al. (2005)	N/A	Atacama Desert, Chile	Soil	+9.03
Jackson et al. (2021)	AT11-100	Atacama Desert, Chile	Soil	+9.0
Jackson et al. (2010)	P3	Atacama Desert, Chile	Soil	+8.8

Jackson et al. (2010)	UIC 24 (J-470)	Atacama Desert, Chile	Soil	+8.8
Böhlke et al. (2005)	N/A	Atacama Desert, Chile	Soil	+8.7
Jackson et al. (2010)	Confidence Hills 1	Death Valley, USA	Soil	+8.6
Hatzinger et al. (2018)	1S/4W-18G1	Rialto-Colton Subbasin, CA, USA	Groundwater	+8.6
Jackson et al. (2010)	P4	Atacama Desert, Chile	Soil	+8.5
Böhlke et al. (2009)	DL6d	Long Island, NY, USA	Groundwater	+8.4
Sturchio et al. (2012)	Well 9	San Bernardino Basin, CA, USA	Groundwater	+8.3
Sturchio et al. (2012)	Well 18	San Bernardino Basin, CA, USA	Groundwater	+8.2
Böhlke et al. (2009)	DL1d	Long Island, NY, USA	Groundwater	+8.2
Hatzinger et al. (2018)	1S/6W-23D2	Chino (or Arlington) Subbasins, CA, USA	Groundwater	+8.2
Hatzinger et al. (2018)	1S/6W-23D2	Chino (or Arlington) Subbasins, CA, USA	Groundwater	+8.1
Jackson et al. (2010)	P1	Atacama Desert, Chile	Soil	+8.1
Böhlke et al. (2005)	N/A	Atacama Desert, Chile	Soil	+7.94
Sturchio et al. (2012)	Well 1	San Bernardino Basin, CA, USA	Groundwater	+7.9
Böhlke et al. (2009)	NP4	Long Island, NY, USA	Groundwater	+7.9
Sturchio et al. (2012)	Well 8	San Bernardino Basin, CA, USA	Groundwater	+7.7
Sturchio et al. (2012)	Well 6	San Bernardino Basin, CA, USA	Groundwater	+7.6
Hatzinger et al. (2018)	1S/5W-04N1	Chino (or Arlington) Subbasins, CA, USA	Groundwater	+7.6
Hatzinger et al. (2018)	1S/5W-04N1	Chino (or Arlington) Subbasins, CA, USA	Groundwater	+7.6
Sturchio et al. (2014)	P-05B	Pomona, CA, USA	Groundwater	+7.5
Sturchio et al. (2012)	Well 22	San Bernardino Basin, CA, USA	Groundwater	+7.5
Sturchio et al. (2012)	Well 4	San Bernardino Basin, CA, USA	Groundwater	+7.5
Hatzinger et al. (2018)	1S/5W-14B1	Chino (or Arlington) Subbasins, CA, USA	Groundwater	+7.4
Sturchio et al. (2012)	Well 15	San Bernardino Basin, CA, USA	Groundwater	+7.3
Sturchio et al. (2012)	Well 7	San Bernardino Basin, CA, USA	Groundwater	+7.3
Sturchio et al. (2012)	Well 3	San Bernardino Basin, CA, USA	Groundwater	+7.3

Sturchio et al. (2014)	P-36	Pomona, CA, USA	Groundwater	+7.1
Sturchio et al. (2014)	P-10B	Pomona, CA, USA	Groundwater	+7.1
Hatzinger et al. (2018)	1S/5W-23A1	Chino (or Arlington) Subbasins, CA, USA	Groundwater	+7.1
Jackson et al. (2021)	AT 11-50	Atacama Desert, Chile	Soil	+7.0
Sturchio et al. (2014)	P-07	Pomona, CA, USA	Groundwater	+6.9
Hatzinger et al. (2018)	1S/5W-13B5	Rialto-Colton Subbasin, CA, USA	Groundwater	+6.9
Sturchio et al. (2012)	Well 11	San Bernardino Basin, CA, USA	Groundwater	+6.9
Sturchio et al. (2014)	P-32B	Pomona, CA, USA	Groundwater	+6.9
Sturchio et al. (2014)	P-23	Pomona, CA, USA	Groundwater	+6.8
Sturchio et al. (2014)	P-08B	Pomona, CA, USA	Groundwater	+6.8
Sturchio et al. (2014)	P-15	Pomona, CA, USA	Groundwater	+6.8
Sturchio et al. (2012)	Well 5	San Bernardino Basin, CA, USA	Groundwater	+6.6
Jackson et al. (2021)	AT 10-150	Atacama Desert, Chile	Soil	+6.6
Sturchio et al. (2012)	Well 2	San Bernardino Basin, CA, USA	Groundwater	+6.6
Sturchio et al. (2014)	P-09B	Pomona, CA, USA	Groundwater	+6.5
Sturchio et al. (2014)	P-25	Pomona, CA, USA	Groundwater	+6.5
Sturchio et al. (2014)	P-26	Pomona, CA, USA	Groundwater	+6.5
Sturchio et al. (2014)	P-37	Pomona, CA, USA	Groundwater	+6.5
Hatzinger et al. (2018)	1S/5W-07R1	Chino (or Arlington) Subbasins, CA, USA	Groundwater	+6.4
Hatzinger et al. (2018)	1N/5W-32N1	Chino (or Arlington) Subbasins, CA, USA	Groundwater	+6.2
Hatzinger et al. (2018)	1N/5W-32N1	Chino (or Arlington) Subbasins, CA, USA	Groundwater	+6.1
Hatzinger et al. (2018)	1N/5W-32A1	Rialto-Colton Subbasin, CA, USA	Groundwater	+4.7
Sturchio et al. (2014)	P-21	Pomona, CA, USA	Groundwater	+4.6
Bao & Gu (2004)	AT75-1-KClO4	Atacama Desert, Chile	Soil	+4.2
Sturchio et al. (2012)	Well 12	San Bernardino Basin, CA, USA	Groundwater	+4.0
Hatzinger et al. (2022)	S1	NE Oregon, USA	Groundwater	+3.73
Hatzinger et al. (2018)	1S/5W-05A5	Rialto-Colton Subbasin, CA, USA	Groundwater	+3.4

Hatzinger et al. (2022)	BGW-001	NE Oregon, USA	Groundwater	+2.89
Hatzinger et al. (2018)	1N/5W-33N1	Rialto-Colton Subbasin, CA, USA	Groundwater	+2.8
Poghosyan et al. (2014)	Lake Superior R	Great Lakes	Lakewater	+2.7
Sturchio et al. (2012)	Well 13	San Bernardino Basin, CA, USA	Groundwater	+2.7
Hatzinger et al. (2022)	MW-20	NE Oregon, USA	Groundwater	+2.62
Poghosyan et al. (2014)	Lake Superior P	Great Lakes	Lakewater	+2.6
Poghosyan et al. (2014)	Lake Erie	Great Lakes	Lakewater	+1.8
Hatzinger et al. (2022)	M&P Dairy	NE Oregon, USA	Groundwater	+1.74
Poghosyan et al. (2014)	Lake Ontario	Great Lakes	Lakewater	+1.7
Poghosyan et al. (2014)	Lake Michigan	Great Lakes	Lakewater	+1.7
Poghosyan et al. (2014)	Lake Huron	Great Lakes	Lakewater	+1.6
Cao et al. (2020)	RPY	NE France	Riverwater	+1.3
Jackson et al. (2010)	RR 16	MRGB, New Mexico, USA	Groundwater	+1.3
Hatzinger et al. (2022)	UMCD 11–1	NE Oregon, USA	Groundwater	+1.23
Jackson et al. (2010)	RR-8	MRGB, New Mexico, USA	Groundwater	+1.2
Hatzinger et al. (2018)	1N/5W-17K2	Rialto-Colton Subbasin, CA, USA	Groundwater	+1.2
Hatzinger et al. (2022)	UMCD 11–7	NE Oregon, USA	Groundwater	+1.18
Hatzinger et al. (2018)	1S/5W-02K1	Rialto-Colton Subbasin, CA, USA	Groundwater	+1.0
Jackson et al. (2010)	KJ1	SHP, Texas and New Mexico, USA	Groundwater	+0.8
Sturchio et al. (2012)	Well 20	San Bernardino Basin, CA, USA	Groundwater	+0.8
Jackson et al. (2010)	BW2	SHP, Texas and New Mexico, USA	Groundwater	+0.6
Jackson et al. (2010)	JYT1	SHP, Texas and New Mexico, USA	Groundwater	+0.5
Sturchio et al. (2006)	ORNL-22	West Texas	Groundwater	+0.49
Hatzinger et al. (2022)	POM-15	NE Oregon, USA	Groundwater	+0.43
Sturchio et al. (2006)	ORNL-21	West Texas	Groundwater	+0.42
Sturchio et al. (2012)	Well 10	San Bernardino Basin, CA, USA	Groundwater	+0.4
Jackson et al. (2010)	MW2B	SHP, Texas and New Mexico, USA	Groundwater	+0.3
Jackson et al. (2010)	MW2A	SHP, Texas and New Mexico, USA	Groundwater	+0.3
Jackson et al. (2010)	MW3B	SHP, Texas and New Mexico, USA	Groundwater	+0.3

Sturchio et al. (2012)	Well 16	San Bernardino Basin, CA, USA	Groundwater	+0.3
Jackson et al. (2010)	MW3A	SHP, Texas and New Mexico, USA	Groundwater	+0.3
Sturchio et al. (2012)	Well 19	San Bernardino Basin, CA, USA	Groundwater	+0.3
Hatzinger et al. (2018)	1N/5W-27D1	Rialto-Colton Subbasin, CA, USA	Groundwater	+0.2
Cao et al. (2020)	FVDV	NE France	Groundwater	+0.2
Hatzinger et al. (2018)	1N/5W-33B1	Rialto-Colton Subbasin, CA, USA	Groundwater	+0.2
Jackson et al. (2010)	GW2	SHP, Texas and New Mexico, USA	Groundwater	+0.2
Sturchio et al. (2012)	Well 21	San Bernardino Basin, CA, USA	Groundwater	+0.2
Hatzinger et al. (2018)	1N/5W-29H3	Rialto-Colton Subbasin, CA, USA	Groundwater	+0.2
Cao et al. (2020)	FBN4 (HW)	NE France	Groundwater	+0.2
Hatzinger et al. (2022)	POM-13	NE Oregon, USA	Groundwater	+0.16
Hatzinger et al. (2013)	UMD Flare	University of Massachusetts, Dartmouth, MA, USA	Groundwater	+0.13
Hatzinger et al. (2013)	UMD-8b	University of Massachusetts, Dartmouth, MA, USA	Groundwater	+0.12
Sturchio et al. (2012)	Well 17	San Bernardino Basin, CA, USA	Groundwater	+0.1
Hatzinger et al. (2018)	1N/5W-29H1	Rialto-Colton Subbasin, CA, USA	Groundwater	+0.1
Hatzinger et al. (2018)	1N/5W-21P2	Rialto-Colton Subbasin, CA, USA	Groundwater	+0.1
Böhlke et al. (2009)	BM1	Long Island, NY, USA	Groundwater	+0.1
Hatzinger et al. (2018)	1S/5W-02G1	Rialto-Colton Subbasin, CA, USA	Groundwater	+0.1
Cao et al. (2020)	RM	NE France	Groundwater	+0.1
Hatzinger et al. (2013)	UMD Charge-1	University of Massachusetts, Dartmouth, MA, USA	Groundwater	+0.09
Hatzinger et al. (2013)	UMD Charge-2	University of Massachusetts, Dartmouth, MA, USA	Groundwater	+0.07
Hatzinger et al. (2013)	UMD-7	University of Massachusetts, Dartmouth, MA, USA	Groundwater	+0.06
Hatzinger et al. (2013)	UMD-8a	University of Massachusetts, Dartmouth, MA, USA	Groundwater	+0.05
Sturchio et al. (2006)	ORNL-14	Edwards Airforce Base, CA	Groundwater	+0.04
Sturchio et al. (2006)	ORNL-17	Henderson, NV	Groundwater	+0.02
Sturchio et al. (2012)	Well 23	San Bernardino Basin, CA, USA	Groundwater	0.0

Sturchio et al. (2012)	Well 14	San Bernardino Basin, CA, USA	Groundwater	0.0
Hatzinger et al. (2018)	1N/5W-33B2	Rialto-Colton Subbasin, CA, USA	Groundwater	0.0
Hatzinger et al. (2018)	1N/5W-21N2	Rialto-Colton Subbasin, CA, USA	Groundwater	0.0
Sturchio et al. (2006)	ORNL-16	Las Vegas Wash	Surface water	0.0
Hatzinger et al. (2018)	1S/5W-03A1	Rialto-Colton Subbasin, CA, USA	Groundwater	0.0
Hatzinger et al. (2018)	1N/5W-34B2	Rialto-Colton Subbasin, CA, USA	Groundwater	0.0
Hatzinger et al. (2018)	1N/5W-34B2	Rialto-Colton Subbasin, CA, USA	Groundwater	0.0
Hatzinger et al. (2018)	1N/5W-34G4	Rialto-Colton Subbasin, CA, USA	Groundwater	0.0
Hatzinger et al. (2018)	1N/5W-34M1	Rialto-Colton Subbasin, CA, USA	Groundwater	0.0
Hatzinger et al. (2018)	1N/5W-34M1	Rialto-Colton Subbasin, CA, USA	Groundwater	0.0
Hatzinger et al. (2018)	1S/5W-02B3	Rialto-Colton Subbasin, CA, USA	Groundwater	0.0
Hatzinger et al. (2018)	1S/5W-02G1	Rialto-Colton Subbasin, CA, USA	Groundwater	0.0
Hatzinger et al. (2018)	1N/5W-28J2	Rialto-Colton Subbasin, CA, USA	Groundwater	-0.1
Hatzinger et al. (2018)	1S/5W-02G1	Rialto-Colton Subbasin, CA, USA	Groundwater	-0.1
Böhlke et al. (2009)	BM2	Long Island, NY, USA	Groundwater	-0.1
Cao et al. (2020)	FBN4 (LW)	NE France	Groundwater	-0.3

Notes:

Observations of $\Delta^{17}O(ClO_4^-)$ are compiled from 15 studies (Bao & Gu, 2004; Böhlke et al., 2005, 2009; Cao et al., 2020; Estrada et al., 2021; Hatzinger et al., 2013, 2018, 2022; Jackson et al., 2010, 2016, 2021; Poghosyan et al., 2014; Sturchio et al., 2006, 2012, 2014).

Observations are arranged in the descending order of $\Delta^{17}O(ClO_4^-)$.

All the values are obtained from tables in the main text or supplementary information of these studies except for those from Böhlke et al. (2005) and Estrada et al. (2021). For Böhlke et al. (2005), we extract the measurements from their Figure 1b. For Estrada et al. (2021), the measurements were plotted in their Figure 8.

Table S6. Average $\Delta^{17}O(ClO_4^-$, photochemistry), $\Delta^{17}O(ClO_3)$, and $\Delta^{17}O(OClO)$ weighted by modeled perchlorate-production rate.

	Standard	Using uncorrected $\Delta^{17}O(O_3)$ and $\Delta^{17}O(OH)$ from Brinjikji & Lyons (2021)	Assuming $\Delta^{17}O(OClO) = \Delta^{17}O(O(^3P))$ in the region above 37 km altitude
$\Delta^{17}O(ClO_4^-$, photochemistry)	+ 28.5 ‰	+ 36.9 ‰	+ 26.3 ‰
$\Delta^{17}O(ClO_3)$	+ 33.5 ‰	+ 43.4 ‰	+ 30.6 ‰
$\Delta^{17}O(OClO)$	+ 48.3 ‰	+ 62.6 ‰	+ 44.0 ‰

Table S7. Modeled mass of chlorine species and chemical families in the control simulation and main simulation (Unit: Gg Cl). "Total inorganic Cl" refers to the sum of all modeled inorganic chlorine chemical species (Total inorganic Cl (g/p) ≡ HCl (g) + $ClONO_2$ (g) + HOCl (g) + ClO (g) + OClO (g) + ClOO (g) + 2×Cl_2 (g) + Cl (g) + BrCl (g) + ICl (g) + $ClNO_2$ (g) + 2×Cl_2O_2 (g) + 2×Cl_2O_4 (g) + Cl^-(p) + ClO_4^-(p)). Cl_y refers to the gas-phase inorganic chlorine chemical family (i.e., Cl_y (g) = Total inorganic Cl (g/p) – Cl^-(p) – ClO_4^-(p)). ClO_x refers to the gas-phase inorganic oxychlorine chemical family (ClO_x (g) ≡ ClO (g) + OClO (g) + ClOO (g) +ClO_3 (g) + 2×Cl_2O_2 (g) + 2×Cl_2O_4 (g)).

	Stratosphere			**Troposphere**		
Species	**Control**	**+ ClO_3-Cl_2O_4-ClO_4^- chemistry**	**Percentage change (Unit: %)**	**Control**	**+ClO_3-Cl_2O_4-ClO_4^- chemistry**	**Percentage change (Unit: %)**
Total inorganic Cl (g/p)	9.45654E+02	9.45471E+02	-1.93492E-02	2.42111E+03	2.42109E+03	-8.56465E-04
Cl_y (g)	9.44042E+02	9.43860E+02	-1.90032E-01	2.39630E+02	2.39611E+02	-7.83208E-03
ClO_x (g)	4.257E+01	4.248E+01	-2.106E-01	4.316E-01	4.311E-01	-1.144E-01
HCl (g)	6.232E+02	6.219E+02	-2.009E-01	2.315E+02	2.314E+02	-3.146E-02
$ClONO_2$ (g)	2.546E+02	2.542E+02	-1.574E-01	1.193E+00	1.192E+00	-1.101E-01
HOCl (g)	1.907E+01	1.904E+01	-1.521E-01	2.192E+00	2.189E+00	-1.152E-01
ClO (g)	3.058E+01	3.052E+01	-1.918E-01	3.052E-01	3.047E-01	-1.776E-01
OClO (g)	1.943E+00	1.941E+00	-9.466E-02	1.224E-01	1.220E-01	-3.030E-01

Table S8. Result of Mann-Whitney U test performed for testing the difference between observed and modeled near-surface [ClO_4^- (p)]

Geographic location	Type of site	Study	Observation data	Model data	Observation median	Model median	Model relative bias in median (%)	U statistic	p-value	Model predictions and observations are distinct at 95% significance level?
Kyoto, Japan	U	Yamada et al. (2009, 2012)	Daily samples, collected from June 2006 to January 2010 (n=131)	Daily average, January 2016 to December 2018 (n=1461)	2.50E-01	7.69E-03	-9.69E+01	190916	1.36E-79	Y
Okinawa, Japan	B	Handa et al. (2010)	Weekly samples, collected from sampled from August 2005 to October 2006 (n=60)	Weekly average, January 2016 to December 2018 (n=209)	1.07E-01	7.38E-03	-9.31E+01	10136	5.34E-34	Y
Lanzhou, China	U	Y. Shi et al. (2011)	12-hourly samples, collected from February to March 2007 (n=25)	12-hourly mean in February and March, from 2016 to 2018 (n=474)	1.98E+00	2.19E-02	-9.89E+01	11766	9.42E-17	Y
Yuzhong County, China	R	Y. Shi et al. (2011)	12-hourly samples, collected from February to March 2007 (n=25)	12-hourly mean in February and March, from 2016 to 2018 (n=474)	1.40E-01	2.40E-02	-8.28E+01	7225	6.44E-02	N

Tokushima, Japan	U	Takeuchi et al. (2012)	3-hourly samples, collected in December 2011 (n=12)	3-hourly mean in December, from 2016 to 2018 (n=992)	4.45E-01	8.36E-03	-9.81E+01	9424	1.4E-128	Y
Lake Toya, Hokkaido, Japan	R	Shirahata (2012)	Monthly samples, collected from Nov 2011 to February 2012 (n=4)	Monthly mean in December, from 2016 to 2018 (n=16)	All below detection limit (0.01 ng m^{-3})	6.90E-03	N/A	26	4.03E-01	N
Jinan, China	U	Yao et al. (2015)	Sampling three times a day from 2013 January 12 to 2013 February 10 (n=67)	8-hourly mean in December and February, from 2016 to 2018 (n=711)	1.47E+00	1.46E-02	-9.90E+01	47637	1.57E-170	Y
Kumamoto, Japan	U	Yao et al. (2015)	72-/96-hourly samples, collected from Nov 2013 to December 2013 (n=7)	72-hourly mean in November and December, from 2016 to 2018 (n=84)	3.96E-02	7.54E-03	-8.10E+01	588	1.23E-05	Y
Changsha, China	U	Wang et al. (2017)	Daily samples, collected from 2016 July 20 to July 31 (n=5)	Daily mean in July, from 2016 to 2018 (n=124)	1.84E+01	2.95E-03	-1.00E+02	620	7.27E-09	Y
Beijing, China	U	H. Zhu et al. (2021)	Daily samples, collected from 2017 March 31 to 2017 April 06 (n=7)	Daily mean in March and April, from 2016 to 2018 (n=244)	3.15E+01	2.36E-02	-9.99E+01	1708	1.75E-13	Y

Tianjin, China	U	H. Zhu et al. (2021)	Daily samples, collected from 2017 March 28 to 2017 April 06 (n=7)	Daily mean in March and April, from 2016 to 2018 (n=244)	2.52E+01	2.34E-02	-9.99E+01	1708	6.59E-06	Y
Zhengzhou, China	U	H. Zhu et al. (2021)	Daily samples, collected from 2017 March 30 to 2017 April 05 (n=7)	Daily mean in March and April, from 2016 to 2018 (n=244)	2.27E+01	2.33E-02	-9.99E+01	1708	1.75E-13	Y
Jinan, China	U	H. Zhu et al. (2021)	Daily samples, collected from 2017 March 30 to 2017 April 05 (n=7)	Daily mean in March and April, from 2016 to 2018 (n=244)	2.03E+01	2.33E-02	-9.99E+01	1708	1.75E-13	Y
Baoding, China	U	H. Zhu et al. (2021)	Daily samples, collected from 2017 March 30 to 2017 April 06 (n=7)	Daily mean in March and April, from 2016 to 2018 (n=244)	4.41E+01	2.36E-02	-9.99E+01	1708	1.75E-13	Y
Shijazhuang, China	U	H. Zhu et al. (2021)	Daily samples, collected from 2017 March 31 to 2017 April 06 (n=7)	Daily mean in March and April, from 2016 to 2018 (n=244)	1.50E+01	2.36E-02	-9.98E+01	1708	1.75E-13	Y
Longgang, Shenzhen, China	U	Zheng et al. (2022)	Monthly mean from October 2020 to September 2021 (n=12)	Monthly mean from January 2016 to December 2018 (n=48)	5.13E-02	5.53E-03	-8.92E+01	551	1.23E-06	Y

Nanshan, Shenzhen, China	U	Zheng et al. (2022)	Monthly mean from October 2020 to September 2021 (n=12)	Monthly mean from January 2016 to December 2018 (n=48)	5.03E-02	5.53E-03	-8.90E+01	560	5.24E-07	Y
Yantian, Shenzhen, China	U	Zheng et al. (2022)	Monthly mean from October 2020 to September 2021 (n=12)	Monthly mean from January 2016 to December 2018 (n=48)	5.24E-02	5.53E-03	-8.94E+01	568	2.4E-07	Y
Open-ocean region sampled by the research cruise from Shanghai to Antarctica	B	Jiang et al. (2021)	24-to-72-hourly sample collected from November 2015 to December 2012 and from March 2016 to April 2016 (n=22)	Modeled value at the location and the sampling period of the observations (n=22)	3.40E-02	2.65E-03	-9.22E+01	471	8.14E-08	Y
Near-coast region sampled by the research cruise from Shanghai to Antarctica	B	Jiang et al. (2021)	24-to-72-hourly sample collected from November 2015 to December 2012 and from March 2016 to April 2016 (n=20)	Modeled value at the location and the sampling period of the observations (n=20)	1.00E-01	4.38E-03	-9.56E+01	335	2.74E-04	Y

Antarctica	B	Jiang et al. (2021)	24-to-72-hourly or 7-day samples collected from December 2015 to February 2016 (n=34)	Modeled value at the location and the sampling period of the observations (n=34)	1.34E-01	1.16E-02	-9.14E+01	1156	1.4E-12	Y

Site types: Urban (U), Rural (R), Background (B).

Table S9. Modeled global perchlorate production in 2016 in the main simulation and ClO_3-photolysis experiments

	Main simulation	ClO_3-photolysis experiment, UV absorption band only	(c) ClO_3-photolysis experiment, whole absorption band
Global perchlorate production in 2016 (Gg/ year)	1.67	0.28	0.05
Production ratio (without ClO_3 photolysis/ with ClO_3 photolysis)	N/A	6.0	30.5

References

Alexander, B., Park, R. J., Jacob, D. J., Li, Q. B., Yantosca, R. M., Savarino, J., et al. (2005). Sulfate formation in sea-salt aerosols: Constraints from oxygen isotopes. *Journal of Geophysical Research: Atmospheres*, *110*(D10). https://doi.org/10.1029/2004JD005659

Alexander, B., Allman, D. J., Amos, H. M., Fairlie, T. D., Dachs, J., Hegg, D. A., & Sletten, R. S. (2012). Isotopic constraints on the formation pathways of sulfate aerosol in the marine boundary layer of the subtropical northeast Atlantic Ocean. *Journal of Geophysical Research: Atmospheres*, *117*(D6). https://doi.org/10.1029/2011JD016773

Alexander, B., Sherwen, T., Holmes, C. D., Fisher, J. A., Chen, Q., Evans, M. J., & Kasibhatla, P. (2020). Global inorganic nitrate production mechanisms: comparison of a global model with nitrate isotope observations. *Atmospheric Chemistry and Physics*, *20*(6), 3859–3877. https://doi.org/10.5194/acp-20-3859-2020

Ali, M. A., & Rajakumar, B. (2011). Thermodynamic and kinetic studies of hydroxyl radical reaction with bromine oxide using density functional theory. *Computational and Theoretical Chemistry*, *964*(1), 283–290. https://doi.org/10.1016/j.comptc.2011.01.013

Andraski, B. J., Jackson, W. A., Welborn, T. L., Böhlke, J. K., Sevanthi, R., & Stonestrom, D. A. (2014). Soil, plant, and terrain effects on natural perchlorate distribution in a desert landscape. *Journal of Environmental Quality*, *43*(3), 980–994. https://doi.org/10.2134/jeq2013.11.0453

Bao, H., & Gu, B. (2004). Natural perchlorate has a unique oxygen isotope signature. *Environmental Science and Technology*, *38*(19), 5073–5077. https://doi.org/10.1021/es049516z

Barron, L., Nesterenko, P. N., & Paull, B. (2006). Rapid on-line preconcentration and suppressed micro-bore ion chromatography of part per trillion levels of perchlorate in rainwater samples. *Analytica Chimica Acta*, *567*(1), 127–134. https://doi.org/10.1016/j.aca.2006.01.038

Begović, N., Marković, Z., Anić, S., & Kolar-Anić, L. (2004). Computational Investigation of HIO and HIO2 Isomers. *The Journal of Physical Chemistry A*, *108*(4), 651–657. https://doi.org/10.1021/jp034492o

Böhlke, J. K., Sturchio, N. C., Gu, B., Horita, J., Brown, G. M., Jackson, W. A., et al. (2005). Perchlorate isotope forensics. *Analytical Chemistry*, *77*(23), 7838–7842. https://doi.org/10.1021/ac051360d

Böhlke, J. K., Hatzinger, P. B., Sturchio, N. C., Gu, B., Abbene, I., & Mroczkowski, S. J. (2009). Atacama perchlorate as an agricultural contaminant in groundwater: Isotopic and chronologic evidence from Long Island, New York. *Environmental Science and Technology*, *43*(15), 5619–5625. https://doi.org/10.1021/es9006433

Brasseur, G. P., & Solomon, S. (2005). *Aeronomy of the Middle Atmosphere: Chemistry and Physics of the Stratosphere and Mesosphere* (Vol. 32). Dordrecht: Springer Netherlands. https://doi.org/10.1007/1-4020-3824-0

Brinjikji, M., & Lyons, J. R. (2021). Mass-Independent Fractionation of Oxygen Isotopes in the Atmosphere. *Reviews in Mineralogy and Geochemistry*, *86*(1), 197–216. https://doi.org/10.2138/rmg.2021.86.06

Burkholder, J. B., Sander, S. P., Abbatt, J. P. D., Barker, J. R., Cappa, C., Crounse, J. D., et al. (2020). *Chemical kinetics and photochemical data for use in atmospheric studies; evaluation number 19*. Pasadena, CA, USA: Jet Propulsion Laboratory. Retrieved from http://hdl.handle.net/2014/49199

Cao, F., Sturchio, N. C., Ollivier, P., Devau, N., Heraty, L. J., & Jaunat, J. (2020). Sources and behavior of perchlorate in a shallow Chalk aquifer under military (World War I) and agricultural influences. *Journal of Hazardous Materials*, *398*, 123072. https://doi.org/10.1016/j.jhazmat.2020.123072

Catling, D. C., Claire, M. W., Zahnle, K. J., Quinn, R. C., Clark, B. C., Hecht, M. H., & Kounaves, S. (2010). Atmospheric origins of perchlorate on Mars and in the Atacama. *Journal of Geophysical Research*, *115*(E1), E00E11. https://doi.org/10.1029/2009JE003425

Cole-Dai, J., Peterson, K. M., Kennedy, J. A., Cox, T. S., & Ferris, D. G. (2018). Evidence of Influence of Human Activities and Volcanic Eruptions on Environmental Perchlorate from a 300-Year Greenland Ice Core Record. *Environmental Science & Technology*, *52*(15), 8373–8380. https://doi.org/10.1021/acs.est.8b01890

Coy, L., Wargan, K., Molod, A. M., McCarty, W. R., & Pawson, S. (2016). Structure and Dynamics of the Quasi-Biennial Oscillation in MERRA-2. *Journal of Climate*, *29*(14), 5339–5354. https://doi.org/10.1175/JCLI-D-15-0809.1

Crawford, T. Z., Kub, A. D., Peterson, K. M., Cox, T. S., & Cole-Dai, J. (2017). Reduced perchlorate in West Antarctica snow during stratospheric ozone hole. *Antarctic Science*, *29*(3), 292–296. https://doi.org/10.1017/S0954102016000705

Dasgupta, P. K., Martinelango, P. K., Jackson, W. A., Anderson, T. A., Tian, K., Tock, R. W., & Rajagopalan, S. (2005). The origin of naturally occurring perchlorate: The role of atmospheric processes. *Environmental Science and Technology*, *39*(6), 1569–1575. https://doi.org/10.1021/es048612x

Domae, M., Katsumara, Y., Jiang, P. Y., Nagaishi, R., Hasegawa, C., Ishigure, K., & Yoshida, Y. (1994). Observation of chlorine oxide (ClO3) radical in aqueous chlorate solution by pulse radiolysis. The Journal of Physical Chemistry, 98(1), 190–192. https://doi.org/10.1021/j100052a031

Du, Z., Xiao, C., Furdui, V. I., & Zhang, W. (2019). The perchlorate record during 1956–2004 from Tienshan ice core, East Asia. *Science of The Total Environment*, *656*, 1121–1132. https://doi.org/10.1016/J.SCITOTENV.2018.11.456

Dubey, M. K., Mohrschladt, R., Donahue, N. M., & Anderson, J. G. (1997). Isotope Specific Kinetics of Hydroxyl Radical (OH) with Water (H2O): Testing Models of Reactivity and Atmospheric Fractionation. *The Journal of Physical Chemistry A*, *101*(8), 1494–1500. https://doi.org/10.1021/jp962332p

Eastham, S. D., Weisenstein, D. K., & Barrett, S. R. H. (2014). Development and evaluation of the unified tropospheric–stratospheric chemistry extension (UCX) for the global chemistry-transport model GEOS-Chem. *Atmospheric Environment*, *89*, 52–63. https://doi.org/10.1016/j.atmosenv.2014.02.001

Eastham, S. D., Fritz, T., Sanz-Morère, I., Prashanth, P., Allroggen, F., Prinn, R. G., et al. (2022). Impacts of a near-future supersonic aircraft fleet on atmospheric composition and climate. *Environmental Science: Atmospheres*, *2*(3), 388–403. https://doi.org/10.1039/D1EA00081K

Emerson, E. W., Hodshire, A. L., DeBolt, H. M., Bilsback, K. R., Pierce, J. R., McMeeking, G. R., & Farmer, D. K. (2020). Revisiting particle dry deposition and its role in radiative effect estimates. *Proceedings of the National Academy of Sciences*, *117*(42), 26076–26082. https://doi.org/10.1073/pnas.2014761117

Estrada, N. L., Anderson, T. A., Böhlke, J. K., Gu, B., Hatzinger, P. B., Mroczkowski, S. J., et al. (2021). Origin of the isotopic composition of natural perchlorate: Experimental results for the impact of reaction pathway and initial ClOx reactant. *Geochimica et Cosmochimica Acta*, *311*, 292–315. https://doi.org/10.1016/j.gca.2021.06.039

Francisco, J. S. (1998). Oxygen atom exchange in reactions of OH radicals with NO and ClO. *Chemical Physics Letters*, *285*(1), 138–142. https://doi.org/10.1016/S0009-2614(98)00010-4

Furdui, V. I., & Tomassini, F. (2010). Trends and sources of perchlorate in Arctic snow. *Environmental Science and Technology*, *44*(2), 588–592. https://doi.org/10.1021/es902243b

Furdui, V. I., Zheng, J., & Furdui, A. (2018). Anthropogenic Perchlorate Increases since 1980 in the Canadian High Arctic. *Environmental Science & Technology*, *52*(3), 972–981. https://doi.org/10.1021/acs.est.7b03132

Fussen, D., Vanhellemont, F., Dodion, J., Bingen, C., Mateshvili, N., Daerden, F., et al. (2006). A global OClO stratospheric layer discovered in GOMOS stellar occultation measurements. *Geophysical Research Letters*, *33*(13). https://doi.org/10.1029/2006GL026406

Gan, Z., Sun, H., Wang, R., & Deng, Y. (2014). Occurrence and exposure evaluation of

perchlorate in outdoor dust and soil in mainland China. *Science of The Total Environment*, *470–471*, 99–106. https://doi.org/10.1016/j.scitotenv.2013.09.067

Gelaro, R., McCarty, W., Suárez, M. J., Todling, R., Molod, A., Takacs, L., et al. (2017). The Modern-Era Retrospective Analysis for Research and Applications, Version 2 (MERRA-2). *Journal of Climate*, *30*(14), 5419–5454. https://doi.org/10.1175/JCLI-D-16-0758.1

Goodeve, C. F., & Richardson, F. D. (1937). The absorption spectrum of chlorine trioxide and chlorine hexoxide. *Transactions of the Faraday Society*, *33*(0), 453–457. https://doi.org/10.1039/TF9373300453

Green, T. J., Islam, M., Canosa-Mas, C., Marston, G., & Wayne, R. P. (2004). Higher oxides of chlorine: Absorption cross-sections of Cl2O6 and C12O4, the decomposition of Cl2O6, and the reactions of OClO with O and O3. *Journal of Photochemistry and Photobiology A: Chemistry*, *162*(2–3), 353–370. https://doi.org/10.1016/S1010-6030(03)00379-4

Greenblatt, G. D., & Howard, C. J. (1989). Oxygen atom exchange in the interaction of hydroxyl-(18OH) with several small molecules. *The Journal of Physical Chemistry*, *93*(3), 1035–1042. https://doi.org/10.1021/j100340a006

Grothe, H., & Willner, H. (1994). Chlortrioxid: spektroskopische Eigenschaften, Molekülstruktur und photochemisches Verhalten. Angewandte Chemie, 106(14), 1581–1583. https://doi.org/10.1002/ange.19941061433

Handa, D., Okada, K., Nakajima, H., & Arakaki, T. (2010). Perchlorate Ion in Aerosols Collected at Cape Hedo, Okinawa, Japan. *Earozoru Kenkyu*, *25*(3), 269–273. https://doi.org/10.11203/jar.25.269

Hathorn, B. C., & Marcus, R. A. (1999). An intramolecular theory of the mass-independent isotope effect for ozone. I. *The Journal of Chemical Physics*, *111*(9), 4087–4100. https://doi.org/10.1063/1.480267

Hatzinger, P. B., Böhlke, J. K., Sturchio, N. C., & Gu, B. (2013). Validation of Chlorine and Oxygen Isotope Ratios to Differentiate Perchlorate Sources and Document Perchlorate Biodegradation (Final Report). Environmental Security Technology Certification Program. Retrieved from http://www.serdp.org/Program-Areas/Environmental-Restoration/Contaminated-Groundwater/Emerging-Issues/ER-200509

Hatzinger, P. B., Böhlke, J. K., Sturchio, N. C., Izbicki, J., & Teague, N. (2018). Four-dimensional isotopic approach to identify perchlorate sources in groundwater: Application to the Rialto-Colton and Chino subbasins, southern California (USA). *Applied Geochemistry*, *97*, 213–225. https://doi.org/10.1016/j.apgeochem.2018.08.020

Hatzinger, P. B., Böhlke, J. K., Jackson, W. A., Gu, B., Mroczkowski, S. J., & Sturchio, N. C. (2022). Isotopic discrimination of natural and anthropogenic perchlorate sources in groundwater in a semi-arid region of northeastern Oregon (USA). *Applied Geochemistry*, *139*, 105232. https://doi.org/10.1016/j.apgeochem.2022.105232

Hegglin, M. I., Tegtmeier, S., Anderson, J., Bourassa, A. E., Brohede, S., Degenstein, D., et al. (2021). Overview and update of the SPARC Data Initiative: comparison of stratospheric composition measurements from satellite limb sounders. *Earth System Science Data*, *13*(5), 1855–1903. https://doi.org/10.5194/essd-13-1855-

2021

Heidenreich, J. E., & Thiemens, M. H. (1986). A non-mass-dependent oxygen isotope effect in the production of ozone from molecular oxygen: The role of molecular symmetry in isotope chemistry. *The Journal of Chemical Physics*, *84*(4), 2129–2136. https://doi.org/10.1063/1.450373

Helsel, D. R. (2013). *Statistics for censored environmental data using minitab and r*. Hoboken, N.J.: Wiley.

Hoering, T. C., Ishimori, F. T., & McDonald, H. O. (1958). The Oxygen Exchange Between Oxy-anions and Water. II. Chlorite, Chlorate and Perchlorate Ions [1]. *Journal of the American Chemical Society*, *80*(15), 3876–3879. https://doi.org/10.1021/ja01548a020

Hoesly, R. M., Smith, S. J., Feng, L., Klimont, Z., Janssens-Maenhout, G., Pitkanen, T., et al. (2018). Historical (1750–2014) anthropogenic emissions of reactive gases and aerosols from the Community Emissions Data System (CEDS). *Geoscientific Model Development*, *11*(1), 369–408. https://doi.org/10.5194/gmd-11-369-2018

Ishino, S., Hattori, S., Savarino, J., Jourdain, B., Preunkert, S., Legrand, M., et al. (2017). Seasonal variations of triple oxygen isotopic compositions of atmospheric sulfate, nitrate, and ozone at Dumont d'Urville, coastal Antarctica. *Atmospheric Chemistry and Physics*, *17*(5), 3713–3727. https://doi.org/10.5194/acp-17-3713-2017

Jackson, W. A., Karl Böhlke, J., Gu, B., Hatzinger, P. B., & Sturchio, N. C. (2010). Isotopic composition and origin of indigenous natural perchlorate and co-occurring nitrate in the southwestern united states. *Environmental Science and*

Technology, *44*(13), 4869–4876. https://doi.org/10.1021/es903802j

Jackson, W. A., Davila, A. F., Böhlke, J. K., Sturchio, N. C., Sevanthi, R., Estrada, N., et al. (2016). Deposition, accumulation, and alteration of Cl-, NO3-, ClO4- and ClO3- salts in a hyper-arid polar environment: Mass balance and isotopic constraints. *Geochimica et Cosmochimica Acta*, *182*, 197–215. https://doi.org/10.1016/j.gca.2016.03.012

Jackson, W. A., Brundrett, M., Böhlke, J. K., Hatzinger, P. B., Mroczkowski, S. J., & Sturchio, N. C. (2021). Isotopic composition of natural and synthetic chlorate (δ18O, Δ17O, δ37Cl, 36Cl/Cl): Methods and initial results. *Chemosphere*, *274*, 129586. https://doi.org/10.1016/j.chemosphere.2021.129586

Jaeglé, L., Quinn, P. K., Bates, T. S., Alexander, B., & Lin, J.-T. (2011). Global distribution of sea salt aerosols: new constraints from in situ and remote sensing observations. *Atmospheric Chemistry and Physics*, *11*(7), 3137–3157. https://doi.org/10.5194/acp-11-3137-2011

Jiang, S., Cox, T. S., Cole-Dai, J., Peterson, K. M., & Shi, G. (2016). Trends of perchlorate in Antarctic snow: Implications for atmospheric production and preservation in snow. *Geophysical Research Letters*, *43*(18), 9913–9919. https://doi.org/10.1002/2016GL070203

Jiang, S., Cole-Dai, J., An, C., Shi, G., Yu, J., & Sun, B. (2020). Spatial variability of perchlorate in East Antarctic surface snow: Implications for atmospheric production. *Atmospheric Environment*, 117743. https://doi.org/10.1016/j.atmosenv.2020.117743

Jiang, S., Shi, G., Cole-Dai, J., An, C., & Sun, B. (2021). Occurrence, latitudinal gradient

and potential sources of perchlorate in the atmosphere across the hemispheres (31°N to 80°S). *Environment International*, *156*, 106611. https://doi.org/10.1016/j.envint.2021.106611

Kannan, K., Praamsma, M. L., Oldi, J. F., Kunisue, T., & Sinha, R. K. (2009). Occurrence of perchlorate in drinking water, groundwater, surface water and human saliva from India. *Chemosphere*, *76*(1), 22–26. https://doi.org/10.1016/j.chemosphere.2009.02.054

Kent Murmann, R., & Thompson, R. C. (1970). Exchange between aqueous ClO2 and H2O. *Journal of Inorganic and Nuclear Chemistry*, *32*(4), 1404–1406. https://doi.org/10.1016/0022-1902(70)80147-6

Knowland, K. E., Keller, C. A., Wales, P. A., Wargan, K., Coy, L., Johnson, M. S., et al. (2022). NASA GEOS Composition Forecast Modeling System GEOS-CF v1.0: Stratospheric Composition. *Journal of Advances in Modeling Earth Systems*, *14*(6), e2021MS002852. https://doi.org/10.1029/2021MS002852

Kopitzky, R., Grothe, H., & Willner, H. (2002). Chlorine Oxide Radicals ClOx (x=1–4) Studied by Matrix Isolation Spectroscopy. Chemistry – A European Journal, 8(24), 5601–5621. https://doi.org/10.1002/1521-3765(20021216)8:24<5601::AID-CHEM5601>3.0.CO;2-Z

Krankowsky, D., Lämmerzahl, P., & Mauersberger, K. (2000). Isotopic measurements of stratospheric ozone. *Geophysical Research Letters*, *27*(17), 2593–2595. https://doi.org/10.1029/2000GL011812

Krankowsky, D., Lämmerzahl, P., Mauersberger, K., Janssen, C., Tuzson, B., & Röckmann, T. (2007). Stratospheric ozone isotope fractionations derived from

collected samples. *Journal of Geophysical Research: Atmospheres*, *112*(D8). https://doi.org/10.1029/2006JD007855

Lämmerzahl, P., Röckmann, T., Brenninkmeijer, C. A. M., Krankowsky, D., & Mauersberger, K. (2002). Oxygen isotope composition of stratospheric carbon dioxide. *Geophysical Research Letters*, *29*(12), 23-1-23–4. https://doi.org/10.1029/2001GL014343

Li, Y., Shen, Y., Pi, L., Hu, W., Chen, M., Luo, Y., et al. (2016). Particle size distribution and perchlorate levels in settled dust from urban roads, parks, and roofs in Chengdu, China. *Environmental Science: Processes & Impacts*, *18*(1), 72–77. https://doi.org/10.1039/C5EM00435G

Li, Y., Liao, R., Gan, Z., Qu, B., Wang, R., Chen, M., et al. (2018). Seasonal Variation and Exposure Risks of Perchlorate in Soil, Indoor Dust, and Outdoor Dust in China. *Archives of Environmental Contamination and Toxicology*, *75*(3), 367–376. https://doi.org/10.1007/s00244-018-0526-x

Lin, J. T., & McElroy, M. B. (2010). Impacts of boundary layer mixing on pollutant vertical profiles in the lower troposphere: Implications to satellite remote sensing. *Atmospheric Environment*, *44*(14), 1726–1739. https://doi.org/10.1016/j.atmosenv.2010.02.009

Lin, S.-J., & Rood, R. B. (1996). Multidimensional Flux-Form Semi-Lagrangian Transport Schemes. *Monthly Weather Review*, *124*(9), 2046–2070. https://doi.org/10.1175/1520-0493(1996)124<2046:MFFSLT>2.0.CO;2

Lin, X., He, L., Zhang, R., Guo, X., & Li, H. (2019). Rainwater in Guangzhou, China: Oxidizing properties and physicochemical characteristics. *Atmospheric Pollution*

Research, *10*(1), 303–312. https://doi.org/10.1016/j.apr.2018.08.005

Liu, H., Jacob, D. J., Bey, I., & Yantosca, R. M. (2001). Constraints from 210 Pb and 7 Be on wet deposition and transport in a global three-dimensional chemical tracer model driven by assimilated meteorological fields. *Journal of Geophysical Research: Atmospheres*, *106*(D11), 12109–12128. https://doi.org/10.1029/2000JD900839

López, M. I., & Sicre, J. E. (1990). Physicochemical properties of chlorine oxides. 1. Composition, ultraviolet spectrum, and kinetics of the thermolysis of gaseous dichlorine hexoxide. *Journal of Physical Chemistry*, *94*(9), 3860–3863. https://doi.org/10.1021/j100372a094

Lyons, J. R. (2001). Transfer of mass-independent fractionation in ozone to other oxygen-containing radicals in the atmosphere. *Geophysical Research Letters*, *28*(17), 3231–3234. https://doi.org/10.1029/2000GL012791

Mauersberger, K., Lämmerzahl, P., & Krankowsky, D. (2001). Stratospheric ozone isotope enrichments—Revisited. *Geophysical Research Letters*, *28*(16), 3155–3158. https://doi.org/10.1029/2001GL013439

Mauldin III, R. L., Burkholder, J. B., & Ravishankara, A. R. (1997). The reaction of O(3P) with OClO. International Journal of Chemical Kinetics, 29(2), 139–147. https://doi.org/10.1002/(SICI)1097-4601(1997)29:2<139::AID-KIN8>3.0.CO;2-V

Meena, G. S., & Devara, P. C. S. (2011). Zenith scattered light measurement: observations of BrO and OClO. *International Journal of Remote Sensing*, *32*(23), 8595–8613. https://doi.org/10.1080/01431161.2010.542621

Meinshausen, M., Vogel, E., Nauels, A., Lorbacher, K., Meinshausen, N., Etheridge, D. M., et al. (2017). Historical greenhouse gas concentrations for climate modelling (CMIP6). *Geoscientific Model Development*, *10*(5), 2057–2116. https://doi.org/10.5194/gmd-10-2057-2017

Michalski, G., & Bhattacharya, S. K. (2009). The role of symmetry in the mass independent isotope effect in ozone. *Proceedings of the National Academy of Sciences*, *106*(14), 5493–5496. https://doi.org/10.1073/pnas.0812755106

Munster, J. (2008, August). *Nonpoint sources of nitrate and perchlorate in urban land use to groundwater, Suffolk County, NY*. Stony Brook University, Stony Brook, NY, USA. Retrieved from http://hdl.handle.net/11401/72036

Munster, J., Hanson, G. N., Jackson, W. A., & Rajagopalan, S. (2009). The Fallout from Fireworks: Perchlorate in Total Deposition. *Water, Air, and Soil Pollution*, *198*(1–4), 149–153. https://doi.org/10.1007/s11270-008-9833-6

Murray, L. T., Jacob, D. J., Logan, J. A., Hudman, R. C., & Koshak, W. J. (2012). Optimized regional and interannual variability of lightning in a global chemical transport model constrained by LIS/OTD satellite data. *Journal of Geophysical Research: Atmospheres*, *117*(D20). https://doi.org/10.1029/2012JD017934

Neu, J. L., Prather, M. J., & Penner, J. E. (2007). Global atmospheric chemistry: Integrating over fractional cloud cover. *Journal of Geophysical Research*, *112*(D11), D11306. https://doi.org/10.1029/2006JD008007

Pace, C., & Vella, A. J. (2019). Contamination of water resources of a small island state by fireworks-derived perchlorate: A case study from Malta. *Environmental Pollution*, *250*, 475–481. https://doi.org/10.1016/j.envpol.2019.04.012

Parrella, J. P., Jacob, D. J., Liang, Q., Zhang, Y., Mickley, L. J., Miller, B., et al. (2012). Tropospheric bromine chemistry: implications for present and pre-industrial ozone and mercury. *Atmospheric Chemistry and Physics*, *12*(15), 6723–6740. https://doi.org/10.5194/acp-12-6723-2012

Poghosyan, A., Sturchio, N. C., Morrison, C. G., Beloso, A. D., Guan, Y., Eiler, J. M., et al. (2014). Perchlorate in the Great Lakes: Isotopic composition and origin. *Environmental Science and Technology*, *48*(19), 11146–11153. https://doi.org/10.1021/es502796d

Pommereau, J.-P., & Piquard, J. (1994). Observations of the vertical distribution of stratospheric OClO. Geophysical Research Letters, 21(13), 1231–1234. https://doi.org/10.1029/94GL00390

Qin, X., Zhang, T., Gan, Z., & Sun, H. (2014). Spatial distribution of perchlorate, iodide and thiocyanate in the aquatic environment of Tianjin, China: Environmental source analysis. *Chemosphere*, *111*, 201–208. https://doi.org/10.1016/j.chemosphere.2014.03.082

Rajagopalan, S., Anderson, T., Cox, S., Harvey, G., Cheng, Q., & Jackson, W. A. (2009). Perchlorate in Wet Deposition Across North America. *Environmental Science & Technology*, *43*(3), 616–622. https://doi.org/10.1021/es801737u

Rao, B. A., Wake, C. P., Anderson, T., & Jackson, W. A. (2012). Perchlorate depositional history as recorded in North American ice cores from the eclipse icefield, Canada, and the Upper Fremont Glacier, USA. *Water, Air, and Soil Pollution*, *223*(1), 181–188. https://doi.org/10.1007/s11270-011-0849-y

Renard, J. B., Lefevre, F., Pirre, M., Robert, C., & Huguenin, D. (1997). Vertical profile

of night-time stratospheric OClO. *Journal of Atmospheric Chemistry*, *26*(1), 65–76. https://doi.org/10.1023/A:1005757321761

Rivière, E. D., Pirre, M., Berthet, G., Renard, J.-B., Taupin, F. G., Huret, N., et al. (2003). On the interaction between nitrogen and halogen species in the Arctic polar vortex during THESEO and THESEO 2000. *Journal of Geophysical Research: Atmospheres*, *107*(D5), SOL 54-1-SOL 54-11. https://doi.org/10.1029/2002JD002087

Rivière, E. D., Pirre, M., Berthet, G., Renard, J.-B., & Lefèvre, F. (2004). Investigating the Halogen Chemistry From High-Latitude Nighttime Stratospheric Measurements of OClO and NO2. *Journal of Atmospheric Chemistry*, *48*(3), 261–282. https://doi.org/10.1023/B:JOCH.0000044423.21004.8e

Ryan, R. G., Marais, E. A., Balhatchet, C. J., & Eastham, S. D. (2022). Impact of Rocket Launch and Space Debris Air Pollutant Emissions on Stratospheric Ozone and Global Climate. *Earth's Future*, *10*(6), e2021EF002612. https://doi.org/10.1029/2021EF002612

Schmidt, J. A., Jacob, D. J., Horowitz, H. M., Hu, L., Sherwen, T., Evans, M. J., et al. (2016). Modeling the observed tropospheric BrO background: Importance of multiphase chemistry and implications for ozone, OH, and mercury. *Journal of Geophysical Research: Atmospheres*, *121*(19). https://doi.org/10.1002/2015JD024229

Schueler, B., Morton, J., & Mauersberger, K. (1990). Measurement of isotopic abundances in collected stratospheric ozone samples. *Geophysical Research Letters*, *17*(9), 1295–1298. https://doi.org/10.1029/GL017i009p01295

Sherwen, T., Evans, M. J., Carpenter, L. J., Andrews, S. J., Lidster, R. T., Dix, B., et al. (2016). Iodine's impact on tropospheric oxidants: a global model study in GEOS-Chem. *Atmospheric Chemistry and Physics*, *16*(2), 1161–1186. https://doi.org/10.5194/acp-16-1161-2016

Sherwen, Tomás, Schmidt, J. A., Evans, M. J., Carpenter, L. J., Großmann, K., Eastham, S. D., et al. (2016). Global impacts of tropospheric halogens (Cl, Br, I) on oxidants and composition in GEOS-Chem. *Atmospheric Chemistry and Physics*, *16*(18), 12239–12271. https://doi.org/10.5194/acp-16-12239-2016

Shi, G., Buffen, A. M., Ma, H., Hu, Z., Sun, B., Li, C., et al. (2018). Distinguishing summertime atmospheric production of nitrate across the East Antarctic Ice Sheet. *Geochimica et Cosmochimica Acta*, *231*, 1–14. https://doi.org/10.1016/j.gca.2018.03.025

Shi, Y., Zhang, N., Gao, J., Li, X., & Cai, Y. (2011). Effect of fireworks display on perchlorate in air aerosols during the Spring Festival. *Atmospheric Environment*, *45*(6), 1323–1327. https://doi.org/10.1016/j.atmosenv.2010.11.056

Shirahata, S. (2012). *Analysis of perchlorate distribution in Lake Toyako* (Master thesis). Rakuno Gakuen University. Retrieved from https://rakuno.repo.nii.ac.jp/?action=pages_view_main&active_action=repository_view_main_item_detail&item_id=3770&item_no=1&page_id=13&block_id=37

Sijimol, M. R., Mohan, M., & Dineep, D. (2016). Perchlorate contamination in bottled and other drinking water sources of Kerala, southwest coast of India. *Energy, Ecology and Environment*, *1*(3), 148–156. https://doi.org/10.1007/s40974-016-0018-7

Simonaitis, R., & Heicklen, J. (1975). Perchloric acid: A possible sink for stratospheric chlorine. *Planetary and Space Science*, *23*(11), 1567–1569. https://doi.org/10.1016/0032-0633(75)90010-0

de Souza, G. L. C., & Brown, A. (2014). Probing ground and low-lying excited states for HIO2 isomers. *The Journal of Chemical Physics*, *141*(23), 234303. https://doi.org/10.1063/1.4903789

Sturchio, N. C., Böhlke, J. K., Gu, B., Horita, J., Brown, G. M., Beloso, A. D., et al. (2006). Stable Isotopic Composition of Chlorine and Oxygen in Synthetic and Natural Perchlorate. In B. Gu & J. D. Coates (Eds.), *Perchlorate: Environmental Occurrence, Interactions and Treatment* (pp. 93–109). Boston, MA: Springer US. https://doi.org/10.1007/0-387-31113-0_5

Sturchio, N. C., Hoaglund, J. R., Marroquin, R. J., Beloso, A. D., Heraty, L. J., Bortz, S. E., & Patterson, T. L. (2012). Isotopic Mapping of Groundwater Perchlorate Plumes. *Ground Water*, *50*(1), 94–102. https://doi.org/10.1111/j.1745-6584.2011.00802.x

Sturchio, N. C., Beloso, A., Heraty, L. J., Wheatcraft, S., & Schumer, R. (2014). Isotopic tracing of perchlorate sources in groundwater from Pomona, California. *Applied Geochemistry*, *43*, 80–87. https://doi.org/10.1016/j.apgeochem.2014.01.012

Takeuchi, M., Yoshioka, K., Toyama, Y., Kagami, A., & Tanaka, H. (2012). On-line measurement of perchlorate in atmospheric aerosol based on ion chromatograph coupled with particle collector and post-column concentrator. *Talanta*, *97*, 527–532. https://doi.org/10.1016/j.talanta.2012.05.009

Thiemens, M. H. (2006). History and Applications of Mass-Independent Isotope Effects.

Annual Review of Earth and Planetary Sciences, *34*(1), 217–262. https://doi.org/10.1146/annurev.earth.34.031405.125026

Tétard, C., Fussen, D., Vanhellemont, F., Bingen, C., Dekemper, E., Mateshvili, N., et al. (2013). OClO slant column densities derived from GOMOS averaged transmittance measurements. Atmospheric Measurement Techniques, 6(11), 2953–2964. https://doi.org/10.5194/amt-6-2953-2013

Van Stempvoort, D. R., MacKay, D. R., Brown, S. J., & Collins, P. (2020). Environmental fluxes of perchlorate in rural catchments, Ontario, Canada. *Science of the Total Environment*, *720*, 137426. https://doi.org/10.1016/j.scitotenv.2020.137426

Vella, A. J., Chircop, C., Micallef, T., & Pace, C. (2015). Perchlorate in dust fall and indoor dust in Malta: An effect of fireworks. *Science of The Total Environment*, *521–522*, 46–51. https://doi.org/10.1016/j.scitotenv.2015.03.071

Vicars, W. C., & Savarino, J. (2014). Quantitative constraints on the 17O-excess (Δ17O) signature of surface ozone: Ambient measurements from 50°N to 50°S using the nitrite-coated filter technique. *Geochimica et Cosmochimica Acta*, *135*, 270–287. https://doi.org/10.1016/j.gca.2014.03.023

Visioni, D., Pitari, G., Tuccella, P., & Curci, G. (2018). Sulfur deposition changes under sulfate geoengineering conditions: quasi-biennial oscillation effects on the transport and lifetime of stratospheric aerosols. *Atmospheric Chemistry and Physics*, *18*(4), 2787–2808. https://doi.org/10.5194/acp-18-2787-2018

Wang, C., Zhai, Y., Zhu, Y., Li, X., Li, C., & Zeng, G. (2017). Concentration and Exposure Evaluation of Perchlorate in Size-Segregated Airborne Particulate

Matter from Changsha, China. *Water, Air, & Soil Pollution*, *228*(9), 369. https://doi.org/10.1007/s11270-017-3555-6

Wang, Q., Jacob, D. J., Spackman, J. R., Perring, A. E., Schwarz, J. P., Moteki, N., et al. (2014). Global budget and radiative forcing of black carbon aerosol: Constraints from pole-to-pole (HIPPO) observations across the Pacific. *Journal of Geophysical Research: Atmospheres*, *119*(1), 195–206. https://doi.org/10.1002/2013JD020824

Wang, X., Jacob, D. J., Downs, W., Zhai, S., Zhu, L., Shah, V., et al. (2021). Global tropospheric halogen (Cl, Br, I) chemistry and its impact on oxidants. *Atmospheric Chemistry and Physics*, *21*(18), 13973–13996. https://doi.org/10.5194/acp-21-13973-2021

Wargan, K., & Coy, L. (2016). Strengthening of the Tropopause Inversion Layer during the 2009 Sudden Stratospheric Warming: A MERRA-2 Study. *Journal of the Atmospheric Sciences*, *73*(5), 1871–1887. https://doi.org/10.1175/JAS-D-15-0333.1

Wargan, K., Labow, G., Frith, S., Pawson, S., Livesey, N., & Partyka, G. (2017). Evaluation of the Ozone Fields in NASA's MERRA-2 Reanalysis. *Journal of Climate*, *30*(8), 2961–2988. https://doi.org/10.1175/JCLI-D-16-0699.1

Wayne, R. P., Poulet, G., Biggs, P., Burrows, J. P., Cox, R. A., Crutzen, P. J., et al. (1995). Halogen oxides: Radicals, sources and reservoirs in the laboratory and in the atmosphere. Atmospheric Environment, 29(20), 2677–2881. https://doi.org/10.1016/1352-2310(95)98124-Q

Wu, S., Mickley, L. J., Jacob, D. J., Logan, J. A., Yantosca, R. M., & Rind, D. (2007).

Why are there large differences between models in global budgets of tropospheric ozone? *Journal of Geophysical Research: Atmospheres*, *112*(D5). https://doi.org/10.1029/2006JD007801

Xu, Z. F., & Lin, M. C. (2003). *Ab initio* studies of ClOx reactions. IX. Combination and disproportionation reactions of ClO and s-ClO3 radicals. *The Journal of Chemical Physics*, *119*(17), 8897–8904. https://doi.org/10.1063/1.1613632

Xu, Z.-F., Zhu, R., & Lin, M. C. (2003). Ab Initio Studies of ClOx Reactions. 3. Kinetics and Mechanism for the OH + OClO Reaction. *The Journal of Physical Chemistry A*, *107*(7), 1040–1049. https://doi.org/10.1021/jp021183+

Yamada, E., Asano, H., & Fuse, Y. (2009). Behavior of Atmospheric Perchlorate in Kyoto City. *BUNSEKI KAGAKU*, *58*(4), 241–247. https://doi.org/10.2116/bunsekikagaku.58.241

Yamada E., Asano H., & Fuse Y. (2012). Environmental Behavior of Perchlorate and its Effect on the Agricultural Products in Kyoto. *Journal of Environment and Safety*, *3*(2), 94–104. https://doi.org/10.11162/daikankyo.3.2_97

Yang, L., Sonk, J. A., & Barker, J. R. (2015). HO + OClO Reaction System: Featuring a Barrierless Entrance Channel with Two Transition States. *The Journal of Physical Chemistry A, 119*(22), 5723–5731. https://doi.org/10.1021/acs.jpca.5b03487

Yao, L., Yang, L., Chen, J., Toda, K., Wang, X., Zhang, J., et al. (2015). Levels, indoor–outdoor relationships and exposure risks of airborne particle-associated perchlorate and chlorate in two urban areas in Eastern Asia. *Chemosphere, 135*, 31–37. https://doi.org/10.1016/j.chemosphere.2015.03.026

Ye, L., You, H., Yao, J., Kang, X., & Tang, L. (2013). Seasonal variation and factors

influencing perchlorate in water, snow, soil and corns in Northeastern China. *Chemosphere*, *90*(10), 2493–2498. https://doi.org/10.1016/j.chemosphere.2012.10.058

Zahn, A., Franz, P., Bechtel, C., Grooß, J.-U., & Röckmann, T. (2006). Modelling the budget of middle atmospheric water vapour isotopes. *Atmospheric Chemistry and Physics*, *6*(8), 2073–2090. https://doi.org/10.5194/acp-6-2073-2006

Zheng, Q., Qiu, H., Zhu, Z., Gong, W., Zhang, D., Ma, J., et al. (2022). Perchlorate in fine particulate matter in Shenzhen, China, and implications for human inhalation exposure. *Environmental Geochemistry and Health*. https://doi.org/10.1007/s10653-022-01381-y

Zhu, H., Qin, X., Xue, L., Zhang, L., & Yuan, M. (2021). Distribution characteristics and health risk assessment of perchlorate in PM2.5 in ambient air from six cities in Beijing-Tianjin-Hebei and its surrounding regions. *Environmental Chemistry*, *40*(9), 2762–2767. https://doi.org/10.7524/j.issn.0254-6108.2020042905

Zhu, R. S., & Lin, M. C. (2001). Ab initio study of ammonium perchlorate combustion initiation processes: Unimolecular decomposition of perchloric acid and the related OH + ClO 3 reaction. *PhysChemComm*, *4*(25), 1–6. https://doi.org/10.1039/b109523b

Zhu, R. S., & Lin, M. C. (2002). Ab Initio Studies of ClO_x Reactions. 2. Unimolecular Decomposition of s-ClO_3 and the Bimolecular O + OClO Reaction. *The Journal of Physical Chemistry A*, *106*(36), 8386–8390. https://doi.org/10.1021/jp020015e

Zhu, R. S., & Lin, M. C. (2003a). Ab initio studies of ClOx reactions. VIII. Isomerization and decomposition of ClO2 radicals and related bimolecular processes. *The*

Journal of Chemical Physics, *119*(4), 2075–2082. https://doi.org/10.1063/1.1585027

Zhu, R. S., & Lin, M. C. (2003b). Towards reliable prediction of kinetics and mechanisms for elementary processes: Key combustion initiation reactions of ammonium perchlorate. In *Theoretical and Computational Chemistry* (Vol. 13, pp. 373–443). Elsevier. https://doi.org/10.1016/S1380-7323(03)80032-8